1 **Transmission dynamics and forecasts of the COVID-19 pandemic in Mexico, March 20-**

2 **November 11, 2020.**

3

4 **Amna Tariq[1], Juan M. Banda[2], Pavel Skums[2], Sushma Dahal[1], Carlos Castillo-Garsow[3],**

5 **Baltazar Espinoza[4], Noel G. Brizuela[5], Roberto A. Saenz[6], Alexander Kirpich[1], Ruiyan**

6 **Luo[1], Anuj Srivastava[7], Humberto Gutierrez[8], Nestor Garcia Chan[8], Ana I. Bento[9], Maria-**

7 **Eugenia Jimenez-Corona[10], Gerardo Chowell[1]**

8

9 [1] Department of Population Health Sciences, School of Public Health, Georgia State University,

10 Atlanta, GA, USA

11 [2] Department of Computer Science, College of Arts and Sciences, Georgia State University,

12 Atlanta, GA, USA

13 [3] Department of Mathematics, Eastern Washington University, Cheney, Washington, USA

14 [4] Biocomplexity Institute and Initiative, Network Systems Science and Advanced Computing

15 Division, University of Virginia, Virginia, USA

16 [5] Scripps Institution of Oceanography, University of California San Diego, La Jolla, CA, USA

17

18 [6] Facultad de Ciencias, Universidad de Colima, Colima, Mexico

19

20 [7] Department of Statistics, Florida State University, Florida, USA

21 [8] Department of Physics, Centro Universitario de Ciencias Exactas e Ingenierias (CUCEI),

22 University of Guadalajara, Guadalajara, Mexico

23 [9] Department of Epidemiology and Biostatistics, School of Public Health, Indiana University

24 Bloomington, Indiana, USA

25 [10] Department of Epidemiology, National Institute of Cardiology "Ignacio Chavez", Mexico City,

26 Mexico

27 * Corresponding author:

1

28   Email: atariq1@student.gsu.edu (AT)

29

30   **Abstract**

31   Mexico has experienced one of the highest COVID-19 death rates in the world. A delayed

32   response towards implementation of social distancing interventions until late March 2020 and a

33   phased reopening of the country in June 2020 has facilitated sustained disease transmission in the

34   region. Here, we systematically generate and compare 30-day ahead forecasts using previously

35   validated growth models based on mortality trends from the Institute for Health Metrics and

36   Evaluation for Mexico and Mexico City in near real-time. Moreover, we estimate reproduction

37   numbers for SARS-CoV-2 based on methods that rely on genomic data as well as case incidence

38   data. Subsequently, functional data analysis techniques are utilized to analyze the shapes of

39   COVID-19 growth rate curves at the state level to characterize the spatial-temporal transmission

40   patterns. The early estimates of reproduction number for Mexico were estimated between R~1.1-

41   1.3 from genomic and case incidence data. Moreover, the mean estimate of R has fluctuated ~1.0

42   from late July till end of September 2020. The spatial analysis characterizes the state-level

43   dynamics of COVID-19 into four groups with distinct epidemic trajectories. We found that the

44   sequential mortality forecasts from the GLM and Richards model predict downward trends in the

45   number of deaths for all thirteen forecasts periods for Mexico and Mexico City. The sub-

46   epidemic and IHME models predict more realistic stable trajectory of COVID-19 mortality

47   trends for the last three forecast periods (09/21-10/21 - 09/28-10/27) for Mexico and Mexico

48   City. Our findings support the view that phenomenological models are useful tools for short-

49   term epidemic forecasting albeit forecasts need to be interpreted with caution given the dynamic

50   implementation and lifting of social distancing measures.

51

Introduction

The ongoing COVID-19 (coronavirus disease 2019) pandemic is the most important global health challenge since the 1918 influenza pandemic [1]. This calls for scientists, health professionals and policy makers to collaboratively address the challenges posed by this deadly infectious disease. The causative SARS-CoV-2 (severe acute respiratory syndrome virus 2) is a novel, unusually complex and highly transmissible virus that spreads via respiratory droplets and aerosols [2, 3]. It presents a clinical spectrum that ranges from asymptomatic individuals to conditions that require the use of mechanical ventilation to multiorgan failure and septic shock leading to death [2]. The ongoing COVID-19 pandemic has not only exerted significant morbidity but also excruciating mortality burden with more than 79.2 million cases and 1.7 million deaths reported worldwide as of December 29, 2020 [4]. Approximately 27 countries globally including 9 countries in the Americas have reported more than 10,000 deaths attributable to SARS-CoV-2 as of December 29, 2020 despite the implementation of social distancing policies to limit the death toll [5]. In comparison, a total of 774 deaths were reported during the 2003 SARS multi-country epidemic and 858 deaths were reported during the 2012 MERS epidemic in Saudi Arabia [6, 7].

Determining the best containment strategies for COVID-19 pandemic is a highly active research area [3]. While multiple vaccines against the novel coronavirus have begun to roll out, many scientific uncertainties exist that will dictate how vaccination campaigns will affect the course of the pandemic. For instance, it is still unclear if the vaccine will prevent the transmission of SARS-CoV-2 or just protect against more severe disease outcomes and death [8, 9]. In these circumstances non-pharmaceutical interventions remain the most promising policy levers to

3

75   reduce the virus transmission [10]. The epidemiological and mathematical models can help

76   quantify the effects of these non-pharmaceutical interventions such as wearing facemasks and

77   social distancing mandates to contain the spread of the virus [11]. However, recent studies have

78   demonstrated that indicators such as population density, poverty, over-crowding and

79   inappropriate work place conditions hinder the social distancing interventions propagating the

80   unmitigated spread of the virus, especially in developing countries [12, 13]. Moreover, the

81   differential mortality trends are also influenced by the disparate disease burden driven by the

82   socioeconomic gradients with the poorest areas showing highest preventable mortality rates [14].

83

84   Mexico, exhibiting one of the highest COVID-19 mortality impact in the world thus far [15], is a

85   highly populated country [16] with ~42% of the population living in poverty (defined as the state

86   if a person or group of people lack a specified amount of money or material possessions) [17]

87   and ~60% of the population work in the informal sector [18]. In this context, Mexico ranks

88   fourth in the world in terms of the number of COVID-19 deaths, a tally surpassed only by the

89   USA, Brazil and India [19] , has reported one of highest death tolls among healthcare workers

90   (~2500 deaths) [20], and has conducted the lowest number of COVID-19 tests per capita [21].

91

92   The Mexican Ministry of Health identified three phases of contingency plan: viral importation,

93   community transmission and epidemic to combat the COVID-19 pandemic in Mexico [22]. The

94   pandemic was likely seeded by imported COVID-19 cases reported on February 28, 2020 [23,

95   24]. As the virus spread across the nation in phase one of the pandemic, some universities

96   switched to virtual classes and some festivals and sporting events were postponed [25].

97   However, the government initially downplayed the impact of the virus and did not enforce strict

98   social distancing measures [26]. This led to large gatherings at some social events such as

99   concerts, festivals and soccer tournament amidst sustained disease transmission in the country

100   [27]. A study conducted in Mexico estimated the early reproduction number for the first ten days

101   of the epidemic between ~2.9-4.9 [28]. However, the true impact of the pandemic was generally

102   under-estimated by the Mexican government despite active virus transmission in the country

103   [29].

104

105   As local clusters of disease started to appear in the community, phase 2 (community

106   transmission) of the pandemic was declared on March 24, 2020 [30]. Authorities suspended all

107   non-essential activities including closure of public and entertainment places and banned

108   gatherings of more than 100 people [31]. This was followed by the declaration of national

109   emergency on March 30, 2020. The new measures to fight the virus under the national

110   emergency included extending the suspension of non-essential activities and a reduction the

111   number of people who can gather to fifty [32]. However, as the virus paved its way across the

112   country ravaging through the poor and rural communities, the government urged the public to

113   comply with the stay-at-home orders [33-35]. These preventive orders from the government were

114   met with mixed reactions from people belonging to different socio-economic sectors of the

115   community [36]. Moreover, transportation restrictions to and from the regions most affected by

116   COVID-19 were not implemented until April 16, 2020 [37]. Shortly after, on April 21, 2020,

117   Mexico announced phase 3 of the contingency (epidemic phase) as wide-spread community

118   transmission intensified [38].

119

120   With lockdowns and other restrictions in place, Mexican officials shared model output [39]

121   predicting that COVID-19 case counts would peak in early May and that the epidemic was

122   expected to end before July 2020 [40]. Despite notorious disagreement between surveillance data

123   and government forecasts, these model predictions continued to be cited by official and

124   independent sources [41, 42]. The extent to which these overly optimistic predictions skewed the

125   plans and budgets of private and public institutions remains unknown. Under the official

126   narrative that the pandemic would soon be over, Mexico planned a gradual phased re-opening of

127   its economy in early June 2020, as the "new normal" phase [43].

128

129   In Mexico, reopening of the economic activities started on June 1 under a four color traffic light

130   monitoring system to alert the residents of the epidemiological risks of COVID-19 based on the

131   level of severity of the pandemic in each state, on a weekly basis [44, 45]. As of December 29,

132   2020 Mexico exhibits high estimates of cumulative COVID-19 cases and deaths; 1,401,529 and

133   123,845 respectively [15]. Given the high transmission potential of the virus and limited

134   application of tests in the country, testing only 24.54 people for every 1000 people (as of

135   December 28, 2020) [21], estimates of the effective reproduction number from the case

136   incidence data and near real-time epidemic projections using mortality data could prove to be

137   highly beneficial to understand the epidemic trajectory of COVID-19. It may also be useful to

138   assess the effect of intervention strategies such as the stay-at-home orders and mobility patterns

139   on the epidemic curve and understand the different spatiotemporal dynamics of the virus.

140

141   In order to investigate the transmission dynamics of the unfolding COVID-19 epidemic in

142   Mexico, we analyze the case data by date of symptoms onset and death data by date of reporting

143 utilizing mathematical models that are useful to characterize the empirical patterns of epidemics

144 [46, 47]. We estimate the effective reproduction number of SARS-CoV-2 in Mexico to

145 understand the transmission dynamics of the virus and examine the mobility trends in relation to

146 the curve of the number of COVID-19 deaths. Moreover, we employ statistical methods from

147 functional data analysis to study the shapes of the COVID-19 growth rate curves at the state

148 level. This helps us characterize the spatial-temporal dynamics of the pandemic based on the

149 shape features of these curves. Lastly, twitter data demonstrating the frequency of tweets

150 indicating stay-at-home-order is analyzed in relation to the COVID-19 case counts at the national

151 level.

152

153 **Methods**

154 **Data**

155 Five sources of data are analyzed in this manuscript. A brief description of the datasets and their

156 sources are described below.

157 **(i)   IHME data for short term forecasts**

158 We utilized the openly published smoothed trend in daily COVID-19 reported deaths from the

159 Institute of Health Metrics and Evaluation (IHME) for (i) Mexico (country) and (ii) Mexico City

160 (capital of Mexico) as of October 9, 2020 to generate the forecasts [48]. IHME smoothed data

161 estimates (current projection scenario) were utilized as they were corrected for the irregularities

162 in the daily death data reporting, by averaging model results over the last seven days. As this was

163 our source of data for prediction modeling, it was chosen for its consistent updates. The

164 statistical procedure of spline regressions obtained from MR-BRT ("meta-regression—Bayesian,

165 regularized, trimmed") smooths the trend in COVID-19 reported deaths as described in ref [10].

166   This data are publicly available from the IHME COVID-19 estimates downloads page [48]. For

167   this analysis, deaths as reported by the IHME model (current projection scenario as described

168   ahead) on November 11, 2020 are used as a proxy for actual reported deaths attributed to

169   COVID-19.

170   **(ii)   Apple mobility trends data**

171   Mobility data for Mexico published publicly by Apple's mobility trends reports was retrieved as

172   of December 5, 2020 [49]. This aggregated and anonymized data is updated daily and includes

173   the relative volume of directions requests per country compared to a baseline volume on January

174   13, 2020. Apple has released the data for the three modes of human mobility: driving, walking

175   and public transit. The mobility measures are normalized in the range 0-100 for each country at

176   the beginning of the series, so trends are relative to this baseline.

177   **(iii)   Case incidence and genomic data for estimating reproduction number**

178   In order to estimate the reproduction number, we use two different data sources. For estimating

179   the early reproduction number from the genomic data, 111 SARS-CoV-2 genome samples were

180   obtained from the "global initiative on sharing avian influenza data" (GISAID) repository

181   between February 27- May 29, 2020 [50]. For estimating the reproduction number from the case

182   incidence data (early reproduction number and the instantaneous reproduction number), we

183   utilized publicly available time series of laboratory-confirmed cases by dates of symptoms onset

184   which were obtained from the Mexican Ministry of Health as of December 5, 2020 [15].

185   **(iv)   Case incidence data for Spatial analysis**

186   We recovered daily case incidence data for all 32 states of Mexico from March 20 to December

187   5 from the Ministry of Health Mexico, as of December 5, 2020 [15].

188   **(v)   Twitter data for twitter analysis**

8

189   For the twitter data analysis, we retrieved data from the publicly available twitter data set of

190   COVID-19 chatter from March 12 to November 11, 2020 [51].

191

192   **Modeling framework for forecast generation**

193   We harness three dynamic phenomenological growth models previously applied to multiple

194   infectious diseases (e.g., SARS, foot and mouth disease, Ebola [52, 53] and the current COVID-

195   19 outbreak [54, 55]) for mortality modeling and short-term forecasting in Mexico and Mexico

196   City. These models include the simple scalar differential equation models such as the generalized

197   logistic growth model [53] and the Richards growth model [56]. We also utilize the sub-

198   epidemic wave model [52] which accommodates complex epidemic trajectories by assembling

199   the contribution of multiple overlapping sub-epidemic waves. The mortality forecasts obtained

200   from these mathematical models can provide valuable insights on the disease transmission

201   mechanisms, the efficacy of intervention strategies and help evaluate optimal resource allocation

202   procedures to inform public health policies. The COVID-19 mortality forecasts for Mexico and

203   Mexico City generated by IHME (current projections scenario) are used as a benchmark model.

204   The description of these models is provided in the supplemental file.

205

206   Cumulative mortality forecasts obtained from our phenomenological growth models are

207   compared with the total mean smoothed death data estimates retrieved from the IHME reference

208   scenario and two IHME counterfactual scenarios. The IHME reference scenario depicts the

209   "current projection", which assumes that the social distancing measures are re-imposed for six

210   weeks whenever daily deaths reach eight per million. The second scenario "mandates easing"

211   implies what would happen if the government continues to ease social distancing measures

212   without re-imposition. Lastly, the third scenario, "universal masks" accounts for universal

213   facemask wearing, that reflects 95% facemask usage in public and social distancing mandates

214   reimposed at 8 deaths per million. Detailed description of these modeling scenarios and their

215   assumptions is explained in ref. [10]. Moreover, the total mean smoothed death data estimates

216   reported by IHME reference scenario as of November 11, 2020 are considered as a proxy for

217   actual death count for each forecasting period.

218

219   **Model calibration and forecasting approach**

220   We conducted 30-day ahead short-term forecasts utilizing thirteen data sets spanned over a

221   period of four months (July 4-October 9, 2020) (Table 1). Each forecast was fitted to the daily

222   death counts from the IHME smoothed data estimates reported between March 20-September 27,

223   2020 for (i) Mexico and (ii) Mexico City. The first model calibration process relies on fifteen

224   weeks of data, from March 20-July 4, 2020. Sequentially models are recalibrated each week with

225   the most up-to-date data, meaning the length of the calibration period increases by one week up

226   to August 2, 2020. However, owing to irregular publishing of data estimates by the IHME, the

227   length of calibration period increased by 2 weeks after August 2, 2020. This was followed by a

228   one week increase from August 17-September 27, 2020 as the data estimates were again

229   published every week.

230

231   Table 1: Characteristics of the data sets used for the sequential calibration and forecasting of the

232   COVID-19 epidemic in Mexico and Mexico City (2020).

Date of the retrieval of data set	Calibration period for the GLM, sub-epidemic, Richards and IHME model	Calibration period (number of days)	Forecast period for the GLM, sub-epidemic, Richards and IHME model
07/04	03/20-07/04	107	07/05-08/03
07/10	03/20-07/11	114	07/12-08/10
07/17	03/20-07/17	120	07/18-08/16
07/27	03/20-07/25	128	07/26-08/24
08/06	03/20-08/02	136	08/03-09/01
08/22	03/20-08/17	151	08/18-09/16
08/27	03/20-08/22	156	08/23-09/21
09/02	03/20-08/30	164	08/31-09/30
09/11	03/20-09/07	172	09/08-10/08
09/18	03/20-09/13	179	09/14-10/13
09/24	03/20-09/20	185	09/21-10/21
10/02	03/20-09/27	193	09/28-10/27
10/09	03/20-09/27	193	09/28-10/27

233
234

235   The 30-day ahead shot-term forecasts generated by calibrating our three phenomenological

236   growth models with the IHME smoothed death data estimates are compared with the forecasts

237   generated by the IHME reference scenario for the same calibration and forecasting periods.

238

239   For each of the three models; GLM, Richards growth model and the sub-epidemic wave model,

240   we estimate the best fit solution for each model using non-linear least square fitting procedure

241   [57]. This process minimizes the sum of squared errors between the model fit, $f(t, \widehat{\Theta})$ and the

242   smoothed data estimates, y_t and yields the best set of parameter estimates $\Theta = (\theta_1, \theta_2, ..., \theta_m)$.

243   The parameters $\widehat{\Theta} = argmin \sum_{t=1}^{n}(f(t,\widehat{\Theta}) - y_t)^2$ define the best fit model $f(t, \Theta)$. Here

244    $\widehat{\Theta} = (r, p, k_o, q \text{ and } C_{thr})$ corresponds to the set of parameters of the sub-epidemic model,

245    $\widehat{\Theta} = (r, k_0, a)$ corresponds to set of parameters of the Richards model and $\widehat{\Theta} = (r, p, k_0)$

246   corresponds to the set of parameters of the GLM model [58]. For the GLM and sub-epidemic

247   wave model, we provide initial best guesses of the parameter estimates. However, for the

248   Richards growth model we initialize the parameters for the nonlinear least squares' method [57]

249   over a wide range of plausible parameters from a uniform distribution using Latin hypercube

250   sampling [59]. This allows us to test the uniqueness of the best fit model. Moreover, the initial

251   conditions are set at the first data point for each of the three models [58]. Uncertainty bounds

252   around the best-fit solution are generated using parametric bootstrap approach with replacement

253   of data assuming a Poisson error structure for the GLM and sub-epidemic model. A negative

254   binomial error structure was used to generate the uncertainty bounds of the Richards growth

255   model; where we assume the mean to be three times the variance based on the noise in the data.

256   Detailed description of this method is provided in ref [58].

257

258   Each of the M best-fit parameter sets are used to construct the 95% confidence intervals for each

259   parameter by refitting the models to each of the M = 300 datasets generated by the bootstrap

260   approach during the calibration phase. Further, each M best fit model solution is used to generate

261   m= 30 additional simulations with Poisson error structure for GLM and sub-epidemic model and

262   negative binomial error structure for Richards model extended through a 30-day forecasting

263   period. For the forecasting period, we construct the 95% prediction intervals with these 9000 (M

264 × m) curves. Detailed description of the methods of parameter estimation can be found in

265 references [58, 60, 61]

266

267 **Performance metrics**

268 We utilized the following four performance metrics to assess the quality of our model fit and the

269 30-day ahead short term forecasts: the mean absolute error (MAE) [62], the mean squared error

270 (MSE) [63], the coverage of the 95% prediction intervals [63], and the mean interval score (MIS)

271 [63] for each of the three models: GLM, Richards model and the sub-epidemic model. For

272 calibration performance, we compare the model fit to the observed smoothed death data

273 estimates fitted to the model, whereas for the performance of forecasts, we compare our forecasts

274 with the smoothed death data estimates (current projections scenario) reported on November 11,

275 2020 for the time period of the forecast.

276 The mean squared error (MSE) and the mean absolute error (MAE) assess the average deviations

277 of the model fit to the observed death data. The mean absolute error (MAE) is given by:

$$MAE = \frac{1}{n} \sum_{i=1}^{n} |f(t_i, \widehat{\Theta}) - y_{t_i}|$$

278 The mean squared error (MSE) is given by:

279

$$MSE = \frac{1}{n} \sum_{i=1}^{n} (f(t_i, \widehat{\Theta}) - y_{t_i})^2$$

13

280   where y_{t_i} is the time series of reported smoothed death estimates, t_i is the time stamp and $\widehat{\Theta}$ is the

281   set of model parameters. For the calibration period, n equals the number of data points used for

282   calibration, and for the forecasting period, $n = 30$ for the 30-day ahead short-term forecast.

283

284   Moreover, in order to assess the model uncertainty and performance of prediction interval, we

285   use the 95% PI and MIS. The prediction coverage is defined as the proportion of observations

286   that fall within 95% prediction interval and is calculated as:

$$PI\ coverage = \frac{1}{n}\sum_{t=1}^{n} I\{Y_t > L_t \cap Y_t < U_t\}$$

287   where Y_t are the smoothed death data estimates, L_t and U_t are the lower and upper bounds of the

288   95% prediction intervals, respectively, n is the length of the period, and I is an indicator variable

289   that equals 1 if value of Y_t is in the specified interval and 0 otherwise

290

291   The mean interval score addresses the width of the prediction interval as well as the coverage.

292   The mean interval score (MIS) is given by:

293

$$MIS = \frac{1}{n}\sum_{i=1}^{n} (U_{t_i} - L_{t_i}) + \frac{2}{0.05}(L_{t_i} - y_{t_i})I\{y_{t_i} < L_{t_i}\} + \frac{2}{0.05}(U_{t_i} - y_{t_i})I\{y_{t_i} > U_{t_i}\}$$

294

295   In this equation L_t, U_t, n and I are as specified above for PI coverage. Therefore, if the PI

296   coverage is 1, the MIS is the average width of the interval across each time point. For two

297   models that have an equivalent PI coverage, a lower value of MIS indicates narrower intervals

298   [63].

14

299

Mobility data analysis

300

301 In order to analyze the time series data for Mexico from March 20-December 5, 2020 for three

302 modes of mobility; driving, walking and public transport, we utilize the R code developed by

303 Kieran Healy [64]. We analyze the mobility trends to look for any pattern in sync with the

304 mortality curve of COVID-19. The time series for mobility requests is decomposed into trends,

305 weekly and remainder components. The trend is a locally weighted regression fitted to the data

306 and remainder is any residual left over on any given day after the underlying trend and normal

307 daily fluctuations have been accounted for.

308

Reproduction number

309

310 We estimate the reproduction number, R_t, for the early ascending phase of the COVID-19

311 epidemic in Mexico and the instantaneous reproduction number R_t throughout the epidemic.

312 Reproduction number, R_t, is a crucial parameter that characterizes the average number of

313 secondary cases generated by a primary case at calendar time t during the outbreak. This

314 quantity is critical to identify the magnitude of public health interventions required to contain an

315 epidemic [65-67]. Estimates of R_t indicate if widespread disease transmission continues ($R_t>1$)

316 or disease transmission declines ($R_t<1$). Therefore, in order to contain an outbreak, it is vital to

317 maintain $R_t<1$.

318

319   **Estimating the reproduction number, R_t, from case incidence using generalized growth**

320   **model (GGM).**

321   We estimate the reproduction number by calibrating the GGM (as described in the supplemental

322   file) to the early growth phase of the epidemic (February 27-May 29, 2020) [68]. The generation

323   interval of SARS-CoV-2 is modeled assuming gamma distribution with a mean of 5.2 days and a

324   standard deviation of 1.72 days [69]. We estimate the growth rate parameter r, and the

325   deceleration of growth parameter p, as described in the supplemental file. The GGM model is

326   used to simulate the progression of local incidence cases I_i at calendar time t_i. This is followed

327   by the application of the discretized probability distribution of the generation interval, denoted

328   by ρ_i, to the renewal equation to estimate the reproduction number at time t_i [70-72]:

329

$$R_{t_i} = \frac{I_i}{\sum_{j=0}^{i}(I_{i-j}\rho_j)}$$

330

331   The numerator represents the total new cases I_i, and the denominator represents the total number

332   of cases that contribute (as primary cases) to generating the new cases I_i (as secondary cases) at

333   time t_i. This way, R_t, represents the average number of secondary cases generated by a single

334   case at calendar time t. The uncertainty bounds around the curve of R_t are derived directly from

335   the uncertainty associated with the parameter estimates (r, p) obtained from the GGM. We

336   estimate R_t for 300 simulated curves assuming a negative binomial error structure [58].

337

338   **Instantaneous reproduction number R_t, using the Cori method.**

339   The instantaneous R_t is estimated by the ratio of number of new infections generated at calendar

340   time t (I_t), to the total infectiousness of infected individuals at time t given by $\sum_{s=1}^{t} I_{t-s} w_s$ [73,

341   74] . Hence R_t can be written as:

$$R_t = \frac{I_t}{\sum_{s=1}^{t} I_{t-s} w_s}$$

342

343   In this equation, I_t is the number of new infections on day t and w_s represents the infectivity

344   function, which is the infectivity profile of the infected individual. This is dependent on the time

345   since infection (s), but is independent of the calendar time (t) [75, 76].

346

347   The term $\sum_{s=1}^{t} I_{t-s} w_s$ describes the sum of infection incidence up to time step $t - 1$, weighted by

348   the infectivity function w_s. The distribution of the generation time can be applied to approximate

349   w_s, however, since the time of infection is a rarely observed event, measuring the distribution of

350   generation time becomes difficult [73]. Therefore, the time of symptom onset is usually used to

351   estimate the distribution of serial interval (SI), which is defined as the time interval between the

352   dates of symptom onset among two successive cases in a disease transmission chain [77].

353

354   The infectiousness of a case is a function of the time since infection, which is proportional to w_s

355   if the timing of infection in the primary case is set as time zero of w_s and we assume that the

356   generation interval equals the SI. The SI was assumed to follow a gamma distribution with a

357   mean of 5.2 days and a standard deviation of 1.72 days [69]. Analytical estimates of R_t were

358   obtained within a Bayesian framework using EpiEstim R package in R language [77]. R_t was

359   estimated at weekly intervals. We reported the median and 95% credible interval (CrI).

360

361   **Estimating the reproduction number, *R*, from the genomic analysis**.

362   In order to estimate the reproduction number for the SARS-CoV-2 between February 27- May

363   29, 2020, from the genomic data, 111 SARS-CoV-2 genomes sampled from infected patients

364   from Mexico and their sampling times were obtained from GISAID repository [50]. Short

365   sequences and sequences with significant number of gaps and non-identified nucleotides were

366   removed, yielding 83 high-quality sequences. For clustering, they were complemented by

367   sequences from other geographical regions, down sampled to n=4325 representative sequences.

368   We used the sequence subsample from Nextstrain (www.nextstrain.org) global analysis as of

369   August 15, 2020. These sequences were aligned to the reference genome taken from the

370   literature [78] using MUSCLE [79] and trimmed to the same length of 29772 bp. The maximum

371   likelihood phylogeny has been constructed using RAxML[80]

372

373   The largest Mexican cluster that possibly corresponds to within-country transmissions has been

374   identified using hierarchical clustering of sequences. The phylodynamics analysis of that cluster

375   have been carried out using BEAST v1.10.4 [81]. We used strict molecular clock and the tree

376   prior with exponential growth coalescent. Markov Chain Monte Carlo sampling has been run for

377   10,000,000 iterations, and the parameters were sampled every 1000 iterations. The exponential

378   growth rate f estimated by BEAST was used to calculate the reproductive number R. For that,

379   we utilized the standard assumption that SARS-CoV-2 generation intervals (times between

380   infection and onward transmission) are gamma-distributed [82]. In that case R can be estimated

381   as $R = \left(1 + \frac{f\sigma^2}{\mu}\right)^{\frac{\mu^2}{\sigma^2}}$, where μ and σ are the mean and standard deviation of that gamma

382   distribution. Their values were taken from ref [69].

383

18

384   **Spatial analysis.**

385   For the shape analysis of incidence rate curves we followed ref. [83] to pre-process the daily

386   cumulative COVID-19 case data at state level as follows:

387   a) Time differencing: If $f_i(t)$ denotes the given cumulative number of confirmed cases for

388   state i on day t, then per day growth rate at time t is given by $g_i(t) = f_i(t) - f_i(t-1)$.

389   b) Smoothing: We then smooth the normalized curves using smooth function in Matlab.

390   c) Rescaling: Rescaling of each curve is done by dividing each g_i by the total confirmed

391   cases for a state i. That is, compute $h_i(t) = g_i(t)/r_i$, where $r_i = \sum_t g_i(t)$.

392   To identify the clusters by comparing the curves, we used a simple metric. For any two

393   rate curves, h_i and h_j, we compute the norm $//h_i - h_j//$, where the double bars denote the L^2

394   norm of the difference function, i.e., $//h_i - h_j// = \sqrt{\sum_t \left(h_i(t) - h_j(t) \right)^2}$.

395   This process is depicted in S17 Fig. To identify the clusters by comparing the curves, we used a

396   simple metric. For any two rate curves, h_i and h_j, we compute the norm $||h_i - h_j||$, where the

397   double bars denote the L^2 norm of the difference function, i.e., $||h_i - h_j|| =$

398    $\sqrt{\sum_t \left(h_i(t) - h_j(t) \right)^2}$. To perform clustering of 32 curves into smaller groups, we apply the

399   dendrogram function in Matlab using the "ward" linkage as explained in ref [84]. The number of

400   clusters is decided empirically based on the display of overall clustering results. After clustering

401   the states into different groups, we derived average curve for each cluster after using a time

402   wrapping algorithm as performed in refs [84, 85].

403

404   **Twitter data analysis.**

19

405   To observe any relationship between the COVID-19 cases by date of symptoms onset and the

406   frequency of tweets indicating stay-at-home orders we used a public dataset of 698 million

407   tweets of COVID-19 chatter [51]. The frequency of tweets indicating stay-at-home order is used

408   to gauge the compliance of people with the orders of staying at home to avoid spread of the virus

409   by maintaining social distance. Tweets indicate the magnitude of the people being pro-lockdown

410   and depict how these numbers have dwindled over the course of the pandemic. To get to the

411   plotted data, we removed all retweets and tweets not in the Spanish language. We also filtered by

412   the following hashtags: #quedateencasa, and #trabajardesdecasa, which are two of the most used

413   hashtags when users refer to the COVID-19 pandemic and their engagement with health

414   measures. Lastly, we limited the tweets to the ones that originated from Mexico, via its 2-code

415   country code: MX. A set of 521,359 unique tweets were gathered from March 12 to November

416   11, 2020. We then overlay the curve of tweets over the epi-curve in Mexico to observe any

417   relation between the shape of the epidemic trajectory and the shape of curve for the frequency of

418   tweets during the established time period. We also estimate the correlation coefficient between

419   the cases and frequency of tweets.

420

421   **Results**

422   As of November 11, 2020, Mexico has reported 105,656 deaths whereas Mexico City has

423   reported 15,742 deaths as per the IHME smoothed death data estimates. Fig 1 (upper panel)

424   shows the daily COVID-19 death curve in Mexico and Mexico City from March 20-November

425   11, 2020. The mobility trend for Mexico (Fig 1, lower panel) shows that the human mobility

426   tracked in the form of walking, driving and public transportation declined from end of March to

427   the beginning of June, corresponding to the implementation of social distancing interventions

428   and the *Jornada Nacional de Sana Distancia* that was put in place between March 23-May 30,

429   2020 encompassing the suspension of non-essential activities in public, private and social sectors

430   [86]. The driving and walking trend subsequently increased in June with the reopening of the

431   non-essential services. Fig 1 (upper panel) shows that reopening of the country coincides with

432   the highest levels of daily deaths. These remain at a high level for just over two months (June

433   and July). Then, from mid-August, the number of deaths begins to fall, reaching a reduction of

434   nearly 50% by mid-October. But at the end of October a new growth begins.

435

436   Fig 1: Upper panel: Epidemic curve for the COVID-19 deaths in Mexico and Mexico City from

437   March 20-November 11, 2020. Blue line depicts the confirmed deaths in Mexico and green line

438   depicts the confirmed deaths in Mexico City.

439   Lower panel: The mobility trends for Mexico from January 1-December 5, 2020. Orange line

440   shows the driving trend, blue line shows the transit trend, and the black line shows the walking

441   trend.

442

443   In the subsequent sections, we first present the results for the short-term forecasting, followed by

444   the estimation of the reproduction numbers. Then we present the results of the spatial analysis

445   and the twitter data analysis.

446

447   **Model calibration and forecasting performance**

448   Here we compare the calibration and 30-day ahead forecasting performance of our three models:

449   the GLM, Richards growth model and the sub-epidemic wave model between March 20-

450   September 27, 2020 and July 5-October 27, 2020 respectively for (i) Mexico and (ii) Mexico

451 City. We also compare the results of our cumulative mortality forecasts with the total mean

452 smoothed death data estimates retrieved from the three IHME model scenarios (as explained in

453 the methods section).

454

455 **Calibration performance.** Across the thirteen sequential model calibration phases for Mexico

456 over a period of seven months (March-September), as provided in Table S1 and Fig 2, the sub-

457 epidemic model outperforms the GLM with lower RMSE estimates for the seven calibration

458 phases 3/20-07/04, 3/20-7/17, 3/20-8/17, 3/20-08/22, 3/20-09/13, 3/20-09/20, 3/20-09/27. The

459 GLM model outperforms the other two models for the remaining six calibration phases in terms

460 of RMSE. The Richards model has substantially higher RMSE (between 10.2-24.9) across all

461 thirteen calibration phases indicating a sub-optimal model fit. The sub-epidemic model also

462 outperforms the other two models in terms of MAE, MIS and the 95% PI coverage. It has the

463 lowest values for MIS and the highest 95% PI coverage for nine of the thirteen calibration phases

464 (Table S1). Moreover, the sub-epidemic model has the lowest MAE for eleven calibration

465 phases. The Richards model shows much higher MIS and lower 95% PI coverage compared to

466 the GLM and sub-epidemic model, pointing towards a sub-optimal model fit.

467

468 Fig 2: Calibration performance for each of the thirteen sequential calibration phases for GLM

469 (magenta), Richards (red) and sub-epidemic (blue) model for Mexico. High 95% PI coverage

470 and lower mean interval score (MIS), root mean square error (RMSE) and mean absolute error

471 (MAE) indicate better performance.

472

473   For Mexico City, the sub-epidemic model outperforms the other two models in terms of all

474   performance metrics. It has the lowest RMSE for eleven of the thirteen calibration phases

475   followed by the GLM and Richards model. The MAE is also the lowest for the sub-epidemic

476   model for all thirteen calibration phases, followed by the GLM and Richards growth model.

477   Further, in terms of MIS, the sub-epidemic model outperforms the Richards and GLM model for

478   nine calibration phases whereas the GLM model outperforms the other two models in four

479   calibration phases (3/20-7/04, 3/20-7/11, 3/20-7/17, 3/20-8/02). The Richards model has much

480   higher estimates for the MIS compared to the other two models indicating a sub-optimal model

481   fit. The 95% PI across all thirteen calibration phases lies between 91.6-99.4% for the sub-

482   epidemic model, followed by the Richards model (85.9- 100%) and the GLM model (53.2-

483   100%) (Table S2, Fig 3).

484

485   Fig 3: Calibration performance for each of the thirteen sequential calibration phases for GLM

486   (magenta), Richards (red) and sub-epidemic (blue) model for Mexico City. High 95% PI

487   coverage and lower mean interval score (MIS), root mean square error (RMSE) and mean

488   absolute error (MAE) indicate better performance.

489

490   Over-all the goodness of fit metrics points toward the sub-epidemic model as the most

491   appropriate model for the Mexico City and Mexico across all four-performance metrics except

492   for the RMSE for Mexico, where the estimates of GLM model compete with the sub-epidemic

493   model.

494

495 **Forecasting performance.** For Mexico, the sub-epidemic model consistently outperforms the

496 GLM and Richards growth model for ten out of the thirteen forecasting phases in terms of RMSE

497 and MAE, eight forecasting phases in terms of MIS and nine forecasting phases in terms of the

498 95% PI coverage. This is followed by the GLM and the Richards growth model (Fig 4, Table

499 S4).

500

501 Fig 4: Forecasting period performance metrics for each of the thirteen sequential forecasting

502 phases for GLM (magenta), Richards (red) and sub-epidemic (blue) model for Mexico. High

503 95% PI coverage and lower mean interval score (MIS), root mean square error (RMSE) and

504 mean absolute error (MAE) indicate better performance.

505

506 Similarly, for Mexico City, the sub-epidemic model consistently outperforms the GLM and

507 Richards growth model for ten of the thirteen forecasting phases in terms of RMSE and MAE

508 and eleven forecasting phases in terms of the MIS. Whereas, in terms of 95% PI coverage,

509 forecasting phases 08/31- 09/29, 09/08-10/08 and 09/21-10/21 show zero 95% PI coverage

510 across all three models. The sub-epidemic model outperforms the Richards and GLM model in

511 six forecasting phases, with the Richards model performing better than the GLM model for the

512 remaining four forecasting phases in terms of the 95% PI coverage (Fig 5, Table S3).

513

514 Fig 5: Forecasting period performance metrics for each of the thirteen sequential forecasting

515 phases for GLM (magenta), Richards (red) and sub-epidemic (blue) model for the Mexico City.

516 High 95% PI coverage and lower mean interval score (MIS), root mean square error (RMSE) and

517 mean absolute error (MAE) indicate better performance.

518

Comparison of daily death forecasts

520   The thirteen sequentially generated daily death forecasts from GLM and Richards growth model,

521   for Mexico and Mexico City indicate towards a sustained decline in the number of deaths (S1

522   Fig, S2 Fig, S3 Fig and S4 Fig). However, the IHME model forecasts (retrieved from smoothed

523   death data estimates, current projections scenario) indicate a decline in the number of deaths for

524   the first six forecasts periods followed by a stable epidemic trajectory for the last seven forecasts,

525   for Mexico City and Mexico. Unlike the GLM and Richards models, the sub-epidemic model is

526   able to reproduce the observed stabilization of daily deaths observed after the first six forecast

527   periods for Mexico and the last three forecast periods for Mexico City (S5 Fig, S6 Fig, S7 Fig

528   and S8 Fig)

529

Comparison of cumulative mortality forecasts

531   The total number of COVID-19 deaths is an important quantity to measure the progression of an

532   epidemic. Here we present the results of the estimated cumulative death counts obtained from

533   our 30-day ahead cumulative forecasts generated using the GLM, Richards and sub-epidemic

534   growth model. We compare these results with the total mean smoothed death data estimates

535   obtained from the three IHME modeling scenarios; current projection, universal masks and

536   mandates easing. The total mean smoothed death data estimates obtained from the IHME current

537   projections scenario as of November 11, 2020 are considered as a proxy for the actual death

538   count for each date that the cumulative forecast is obtained (Figs 6 and 7) .

539

540   Fig 6: Systematic comparison of the six models (GLM, Richards, sub-epidemic model, IHME

541   current projections (IHME C.P), IHME universal masks (IHME U.M) and IHME mandates

542   easing (IHME M.E) to predict the cumulative COVID-19 deaths for Mexico in the thirteen

543   sequential forecasts. The blue circles represent the mean deaths, and the magenta vertical line

544   indicates the 95% PI around the mean death count. The horizontal dashed line represents the

545   actual death count reported by that date in the November 11, 2020 IHME estimates files.

546

547   Fig 7: Systematic comparison of the six (GLM, Richards, sub-epidemic model, IHME current

548   projections (IHME C.P), IHME universal masks (IHME U.M) and IHME mandates easing

549   (IHME M.E) to predict the cumulative COVID-19 deaths for the Mexico City in the thirteen

550   sequential forecasts. The blue circles represent the mean deaths, and the magenta vertical line

551   indicates the 95% PI around the mean death count. The horizontal dashed line represents the

552   actual death count reported by that date in the November 11, 2020 IHME estimates files.

553

554   **Mexico.** The 30-day ahead cumulative forecast results for the thirteen sequentially generated

555   forecasts for Mexico utilizing GLM, Richards growth model, sub-epidemic growth model and

556   the IHME model (current projections scenario) are presented in S9 Fig, S10 Fig, S11 Fig and

557   S12 Fig. The cumulative mortality estimates comparison is given in Fig 6. For the first, second,

558   third and thirteenth generated forecasts the GLM, sub-epidemic model and the Richards model

559   tend to underestimate the true deaths counts (~50,255, ~54,857, ~58,604, 89,730 deaths

560   respectively), whereas the three IHME forecasting scenarios closely estimate the actual death

561   counts for the first, second and thirteenth forecasting periods. For the fourth, fifth and seventh

562   generated forecast the sub-epidemic model and the IHME scenarios most closely approximate

563   the actual death counts (~63,078, ~67,075, ~76,054 deaths respectively). For the sixth generated

564   forecast the GLM model closely approximates the actual death count (~73,911 deaths) whereas

565   for the tenth generated forecast the sub-epidemic model closely approximates the actual deaths

566   (~84,471 deaths). For the eighth, ninth, eleventh and twelfth generated forecast GLM, Richards

567   and sub-epidemic model tend to under-predict the actual death counts with the IHME model

568   underestimating the actual death counts for eleventh and twelfth generated forecast and

569   overestimating the total death counts for the ninth generated forecast (Table 2).

570

571   Table 2: Cumulative mortality estimates obtained from the six models (GLM, Richards model,

572   sub-epidemic model, IHME current projections, IHME universal mask and IHME mandates

573   easing) for each forecasting period of the COVID-19 pandemic in Mexico (2020).

574

Forecast Number	Forecast period	GLM Mean (95% PI)	Sub-epidemic model Mean (95% PI)	Richards model Mean (95% PI)	IHME current projections Mean (95% PI)	IHME universal mask Mean (95% PI)	IHME mandates easing Mean (95% PI)	Actual deaths reported as of Nov 11, 2020
1	07/05-08/03	48,917 (43,931-54,039	48,110 (42,939-53,661)	45,808 (38,808-53,665)	50,721 (47,410-55,597)	49,692 (46,500-54,250)	51,299 (47,893-56,184)	50,255
2	07/12-08/10	49,412 (44,517-49,412)	52,085 (46,973-57,379)	47,358 (39,836-55,808)	54,438 (49,269-59,598)	53,615 (48,634-58,590)	55,176 (49,609-60,621)	54,857
3	07/18-08/16	52,197 (47,059-57,541)	54,758 (49,600-60,070)	50,055 (42,161-58,892)	54,572 (39,989-62,409)	54,020 (39,989-61,614)	54,749 (39,989-62,710)	58,604
4	07/26-08/24	56,658 (51,208-62,320)	62,271 (56,644-68,073)	53,742 (45,332-63,144)	62,902 (58,094-68,253)	62,194 (57,516-67,205)	63,116 (58,285-68,542)	63,078
5	08/03-09/01	61,451 (55,655-67,494)	67,010 (60,988-73,219)	57,186 (48,270-67,114)	66,376 (63,705-69,334)	65,944 (63,308-68,853)	66,582 (63,865-69,612)	67,075
6	08/18-09/16	73,700 (66,996-	79,144 (72,306-	65,814 (55,834-	80,072 (74,140-	79,598 (73,772-	80,537 (74,479-	73,911

		80,655)	86,048)	76,954)	84,710)	84,225)	85,288)	
7	08/23-09/21	73,901 (67,126-80,909)	75,809 (69,107-82,699)	67,273 (57,061-78,667)	75,125 (73,161-78,209)	74,887 (72,993-77,883)	75,160 (73,207-78,254)	76,054
8	08/31-09/30	76,535 (69,509-83,826)	77,629 (70,688-84,743)	70,218 (59,490-82,174)	78,525 (76,644-80,538)	78,653 (76,767-80,669)	79,016 (77,057-81,135)	79,683
9	09/08-10/08	79,406 (72,084-87,022)	79,491 (72,250-86,959)	72,712 (61,556-85,135)	84,215 (80,639-88,038)	84,307 (80,682-88,069)	84,937 (81,130-88,999)	82,669
10	09/14-10/13	81,546 (74,030-89,356)	84,561 (76,905-92,411)	74,504 (63,026-87,292)	86,249 (84,255-88,722)	85,926 (83,982-88,256)	86,249 (84,259-88,694)	84,471
11	09/21-10/21	82,815 (75,098, 90,804)	84,392 (76,640-92,327)	76,386 (64,579-89,556)	84,731 (83,126-86,880)	84,435 (82,872-86,512)	84,731 (83,135-86,864)	87,396
12	09/28-10/27	84,827 (76,896-93,047)	85,885 (77,943-94,022)	78,448 (66,244-92,090)	87,491 (84,095-90,872)	87,265 (83,967-90,580)	87,522 (84,115-90,945)	89,730
13	09/28-10/27	85,197 (77,258-93,454)	86,850 (78,896-95,001)	77,876 (65,750-91,401)	89,666 (88,264-91,036)	89,627 (88,280-91036)	89,667 (88,281-91,036)	89,730

575

576 In summary, the Richards growth model consistently under-estimates the actual death count

577 compared to the GLM, sub-epidemic model and three IHME model scenarios. The GLM model

578 also provides lower estimates of the mean death counts compared to the sub-epidemic and three

579 IHME model scenarios, but higher mean death estimates compared to the Richards model. The

580 95% PI for the Richards model is substantially wider than the other five models indicating wider

581 uncertainty in the results. The actual mean death counts lie within the 95% PI of the sub-

582 epidemic model for all the thirteen forecasts. Moreover, the three IHME model scenarios predict

583 approximately similar cumulative death counts across the thirteen generated forecasts, indicating

584 that the three scenarios do not differ substantially.

585

586   **Mexico City.** The 30 day ahead cumulative forecast results for thirteen sequentially generated

587   forecasts for the Mexico City utilizing GLM, Richards model, sub-epidemic growth model and

588   IHME model (current projections scenario) are presented in S13 Fig, S14 Fig, S15 Fig and S16

589   Fig. The cumulative death comparison is given in Fig 7 and Table 3. For the first generated

590   forecast the sub-epidemic model closely approximates the actual death count (~10,081 deaths).

591   For the second generated forecast, the sub-epidemic model and the IHME scenarios closely

592   approximate the actual death count (~10,496 deaths). For the third and sixth generated forecast

593   GLM and Richards model underestimate the actual death count (~10,859, ~12,615 deaths

594   respectively) whereas the sub-epidemic model closely estimates the death count for the third

595   forecast and under-predicts the death count for the sixth forecast. The three IHME model

596   scenarios seem to predict the actual death counts closely. For the fourth, fifth, seventh, eighth,

597   ninth, tenth, eleventh, twelfth and thirteenth generated forecasts all models under-predict the

598   actual death counts.

599

600   Table 3: Cumulative mortality estimates obtained from the six models (GLM, Richards model,

601   sub-epidemic model, IHME current projections, IHME universal mask and IHME mandates

602   easing) for each forecasting period of the COVID-19 pandemic in Mexico City (2020).

603

Forecast Number	Forecast period	GLM Mean (95% PI)	Sub-epidemic model Mean (95% PI)	Richards model Mean (95% PI)	IHME current projections Mean (95% PI)	IHME universal mask Mean (95% PI)	IHME mandates easing Mean (95% PI)	Actual deaths reported as of Nov 11, 2020
1	07/05-08/03	8,480 (6,642-10,549)	9,655 (7,437-12,016)	8,628 (5,712-12,363)	9,075 (8,334-9,888)	8,991 (8,334-9,888)	9,195 (8,443-10,182)	10,081
2	07/12-	8,968	10,534	9,015	10,091	10,018	10,254	10,496

	08/10	(7,022-11,119)	(8,063-13,187)	(5,951-12,971)	(8,607-12,421)	(8,598-12,263)	(8,648-12,905)	
3	07/18-08/16	9,447 (7,402-11,710)	11,287 (8,541-14,037)	9,495 (6,291-13,616)	10,388 (8,382-12,505)	10,323 (8,381-12,365)	10,467 (8,381-12,660)	10,859
4	07/26-08/24	9,588 (7,478-11,891)	10,249 (8,042-12,622)	9,575 (6,283-13,836)	10,481 (9,761-11,551)	10,424 (9,729-11,433)	10,526 (9,791-11,623)	11,326
5	08/03-09/01	9,786 (7,621-12,166)	10,232 (7,950-12,686)	9,737 (6,351-14,140)	10,314 (9,746-11,477)	10,290 (9,733-11,423)	10,314 (9,746-11,477)	11,769
6	08/18-09/16	10,388 (8,054-12,957)	11,103 (8,646-13,752)	10,425 (6,762-15,212)	12,099 (11,387-13,118)	12,055 (11,362-13,046)	12,184 (11,422-13,255)	12,615
7	08/23-09/21	10,615 (8,226-13,272)	11,205 (8,700-13,911)	10,411 (6,719-15,250)	11,826 (11,289-12,584)	11,794 (11,273-12,527)	11,826 (11,290-12,585)	12,966
8	08/31-09/30	10,851 (8,381-13,581)	11,103 (8,646-13,752)	10,872 (6,997-15,950)	11,829 (11,397-12,328)	11,842 (11,409-12,527)	11,871 (11,421-12,394)	13,414
9	09/08-10/08	11,182 (8,621-14,011)	11,237 (8,721-13,955)	10,820 (6,936-15,966)	12,547 (11,851-13,318)	12,560 (11,859-13,340)	12,604 (11,881-13,413)	13,838
10	09/14-10/13	11,553 (8,887-14,492)	12,443 (9,645-15,439)	11,064 (7,043-16,373)	13,256 (12,586-14,106)	13,215 (12,566-14,031)	13,256 (12,857-14,105)	14,107
11	09/21-10/21	11,711 (8,985-14,714)	12,636 (9,737-15,742)	11,811 (7,578-17,367)	12,727 (12,326-13,200)	12,699 (12,310,13,156)	12,728 (12,327-13,192)	14,561
12	09/28-10/27	12,074 (9,253-15,195)	12,878 (9,919-16,054)	11,503 (7,315-17,079)	13,358 (12,718-14,095)	13,332 (12,705-14,049)	13,361 (12,720-14,153)	14,911
13	09/28-10/27	12,493 (9,570-15,716)	13,460 (10,341-16,815)	11,659 (7,398-17,370)	14,172 (13,539-15,031)	14,131 (13,522-14,958)	14,191 (14,541-15,128)	15,306

604

605

606   In general, the Richards growth model has much wider 95% PI coverage compared to the other

607   models indicating greater uncertainty in the results. The mean cumulative death count estimates

608   for the GLM and Richards model closely approximate each other. However, the actual mean

609   death counts lie within the 95% PI of the GLM and sub-epidemic model for all the thirteen

610 forecasts. The three IHME model scenarios predict approximately similar cumulative death

611 counts across the thirteen generated forecasts with much narrow 95% PI's, indicating that three

612 scenarios do not different substantially.

613

614 **Reproduction number**

615

616 **Estimate of reproduction number, R from genomic data analysis.** The majority of analyzed

617 Mexican SARS-CoV-2 sequences (69 out of 83) have been sampled in March and April 2020.

618 These sequences are spread along the whole global SARS-CoV-2 phylogeny (Fig 8) and split

619 into multiple clusters. This indicates multiple introductions of SARS-CoV-2 to the country

620 during the initial pandemic stage (February 27- May 29, 2020). For the largest cluster of size 42,

621 the reproduction number was estimated at $R = 1.3$ (95% HPD interval [1.1,1.5]).

622

623 Fig 8: Global neighbor-joining tree for SARS-CoV-2 genomic data from February 27- May 29,

624 2020. Sequences sampled in Mexico are highlighted in red.

625

626 **Estimate of reproduction number, R_t from case incidence data.** The reproduction number

627 from the case incidence data (February 27- May 29, 2020) using GGM was estimated at

628 $R_t \sim 1.1$(95% CI:1.1,1.1), in accordance with the estimate of R_t obtained from the genomic data

629 analysis. The growth rate parameter, r, was estimated at 1.2 (95% CI: 1.1, 1.4) and the

630 deceleration of growth parameter, p, was estimated at 0.7 (95% CI: 0.68,0.71), indicating early

631 sub-exponential growth dynamics of the epidemic (Fig 9).

632

633   Fig 9: Upper panel: Reproduction number with 95% CI estimated using the GGM model. The

634   estimated reproduction number of the COVID-19 epidemic in Mexico as of May 29, 2020 is 1.1

635   (95% CI: 1.1, 1.1). The growth rate parameter, r, is estimated at 1.2 (95% CI:1.1, 1.4) and the

636   deceleration of growth parameter, p, is estimated at 0.7 (95% CI:0.68, 0.71).

637   Lower panel: The lower panel shows the GGM fit to the case incidence data for the first 90 days.

638

639   **Estimate of instantaneous reproduction number, R_t.** The instantaneous reproduction number

640   for Mexico remained consistently above 1.0 until the end of May 2020, after which the

641   reproduction number has fluctuated around 1.0 with the estimate of $R_t \sim 0.93$ (95% CrI: 0.91,

642   0.94) as of September 27, 2020. For Mexico City, the reproduction number remained above 1.0

643   until the end of June after which it has fluctuated around 1.0 with the estimate of $R_t \sim 0.96$ (95%

644   CrI: 0.93, 0.99) as of September 27, 2020 (Fig 10).

645

646   Figure 10: Upper panel: Epidemiological curve (by the dates of symptom onset) for Mexico (left

647   panel) and Mexico City (right panel) as of September 27, 2020.

648   Lower panel: Instantaneous reproduction number with 95% credible intervals for the COVID-19

649   epidemic in Mexico as of September 27, 2020. The red solid line represents the mean

650   reproduction number for Mexico and the red shaded area represents the 95% credible interval

651   around it. The blue solid line represents the mean reproduction number for the Mexico City and

652   the blue shaded region represents the 95% credible interval around it.

653

654   **Spatial analysis**

655   Fig S17 shows the result from pre-processing COVID-19 data into growth rate functions. The

656   results of clustering are shown in Fig S18 as a dendrogram plot and the states color coded based

657   on their cluster membership within the map of Mexico (Fig 11; left panel). The four predominant

658   clusters we identified include the following states:

659   Cluster 1: Baja California, Coahuila, Colima, Mexico City, Guanajuato, Guerrero, Hidalgo,

660   Jalisco, Mexico, Michoacán, Morelos, Nuevo Leon, Oaxaca, Puebla, San Luis Potosi, Sinaloa,

661   and Tlaxcala

662   Cluster 2: Baja California Sur, Campeche, Chiapas, Nayarit, Quintana Roo, Sonora, Tabasco,

663   Tamaulipas, Veracruz, and Yucatan

664   Cluster 3: Chihuahua

665   Cluster 4: Aguascalientes, Durango, Queretaro, and Zacatecas

666   Figure 11: Clusters of states by their growth rates. Cluster 1 in blue, cluster 2 in orange, cluster 3

667   in yellow, and cluster 4 in purple. The right panel shows the average growth rate curves for each

668   cluster (solid curves) and their overall average (black broken curve).

669

670   Fig 11(right panel) shows the average shape of growth rate curves in each cluster and the overall

671   average. Fig S19 shows mean growth rate curves and one standard-deviation bands around it, in

672   each cluster. Since cluster 3 included only one state, average growth rate of cluster 1, cluster 2,

673   and cluster 4 are shown. The average growth patterns in the three categories are very distinct and

674   clearly visible. For cluster 1, the rate rises rapidly from April to July and then shows small

675   fluctuations. For cluster 2, there is rapid increase in growth rate from April to July followed by a

676   rapid decline. Chihuahua in cluster 3 shows a slow growth rate until September followed by a

677   rapid rise until mid-September which then declines rapidly. For cluster 4, the rate rises slowly,

678   from April to September, and then shows a rapid rise (Fig S20).

679

680   From the colormap (Fig 12) we can see that the cases were concentrated from the beginning in

681   the central region in Mexico and Mexico City. Daily cases have been square root transformed to

682   reduce variability in the amplitude of the time series while dashed lines separate the Northern,

683   Central, and Southern regions. Fig S20 shows the timeseries graph of daily COVID-19 new cases

684   by the date for all states, Northern states, Central states, and the Southern states. As observed for

685   both Northern and Central regions including the national level, the epidemic peaked in mid-July

686   followed by a decline at around mid-September, which then started rising again. Southern states

687   exhibit a stable decline. Fig S21 shows the total number of COVID-19 cases at state level as of

688   December 5, 2020. Some of the areas with a higher concentration of COVID-19 cases are:

689   Mexico City, Mexico state, Guanajuato in the central region and, Nuevo Leon in the Northern

690   region.

691

692   Fig 12: Color scale image of daily COVID-19 cases by region.

693

694   **Twitter data analysis**

695   The epicurve for Mexico is overlaid with the curve of tweets indicating stay at home orders in

696   Mexico as shown in S22 Fig. The engagement of people in Mexico with the #quedateencasa

697   hashtag (stay-at-home order hashtag) has been gradually declining as the number of cases have

698   continued to increase or remain at a steady pace, showing the frustration and apathy of public on

699   lock downs and restrictions. Mostly the non-government public health experts are calling for

700   more lockdowns or continued social distancing measures (without being heard by the

701   authorities). It could also imply that the population is not following the government's stay at

702   home orders and hence we continue to observe the cases. S22 Fig shows that the highest number

703   of tweets were made in the earlier part of the epidemic, with the number of tweets declining as of

704   mid-May 2020. In contrast, the number of cases by onset dates peaked around mid-June. The

705   correlation coefficient between the epi-curve of cases by dates of onset and the curve of tweets

706   representing the stay-at-home orders was estimated at R=-0.001 from March 12- November 11,

707   2020.

708

709   **Discussion**

710   The results of our GLM model fit to the smoothed death data estimates for all the thirteen

711   calibration phases and GGM fit to the case incidence data indicate sub-exponential growth

712   dynamics of COVID-19 epidemic in the Mexico and Mexico City with the parameter p estimated

713   between (p~0.6-0.8). Moreover, the early estimates of R indicate towards sustained disease

714   transmission in the country. As R_t fluctuates around ~1.0 since the end of July 2020, we observe

715   different epidemic growth patterns at the national and state level. With ongoing virus

716   transmission in Mexico, the Twitter analysis implies the relaxation of lockdowns, with

717   inconsequential decline in the mobility patterns observed over the last few weeks as evident from

718   the Apple's mobility trends. Moreover, the systematic comparison of our models across thirteen

719   sequential forecasts deems sub-epidemic model as the most appropriate model for mortality

720   forecasting. The sub-epidemic model is also able to reproduce the stabilization in the trajectory

721   of mortality forecasts as observed by the IHME forecasts.

722

723   The sub-exponential growth pattern of the COVID-19 epidemic in Mexico can be attributed to a

724   myriad of factors including non-homogenous mixing, spatial structure, population mobility,

725   behavior changes and interventions [87]. Our results are consistent with the sub-exponential

726   growth patterns of COVID-19 outbreaks observed in Mexico [88] and Chile [89]. Along with the

727   observed sub-exponential growth dynamics of the COVID-19 epidemic in Mexico, the

728   reproduction number estimated from the genomic sequence analysis and the case incidence data

729   (R_t~ 1.1-1.2) indicate towards sustained transmission of SARS-CoV-2 in Mexico during the

730   early transmission phase of the virus (February 27- May 29, 2020). Our estimates of R_t are

731   similar to the estimates of reproduction number retrieved from other studies conducted in

732   Mexico [90], Chile [91, 92], Peru [93] and Brazil [94]. The early estimate of R_t obtained from

733   the Cori et al. method in our study also coincides with the early estimates of R_t obtained from

734   the case incidence data and the genomic data (R_t~1). The instantaneous reproduction number

735   estimated from our study shows that R_t is slightly above 1 since the end of March, without a

736   significant increase. This is in accordance with the estimates of R_t obtained from a study

737   conducted in Mexico [95].

738

739   In general, Mexico has seen a sustained SARS-CoV-2 transmission and an increase or a

740   sustained number of cases despite the implementation of the social distancing interventions

741   including the stay-at-home orders that were eased around June 2020. As our twitter data analysis

742   also shows, the number of cases by onset dates was negatively correlated to the stay-at-home

743   orders. A possible explanation indicates that people might have stopped following the

744   government's preventive orders to stay at home as a result of pandemic fatigue [96, 97]. Mexico

745   has been one of the countries where the stay-at-home orders have been least respected. The

746   average reduction in mobility in Mexico is reported to be ~35.4% compared to 71% mobility

747   reduction in Brazil, and 86% mobility reduction in Argentina and Colombia [98]. These

748   preventive orders have affected the Mexican population disproportionately, with some

749   proportion of the population exhibiting aggression towards quarantine and stay-at-home orders

750   [36]. However, the public health professionals are frustrated towards the relaxation of stay-at-

751   home orders and reopening of the country, as the cases and deaths keep mounting. We can also

752   appreciate the variable spatial-temporal dynamics of the COVID-19 epidemic in Mexico. Our

753   classification of epidemic pattern at the state level in Mexico shows distinct variation of growth

754   rates across states. For instance, cluster 1 including Baja California, Colima and Mexico City has

755   stable growth at a higher rate and cluster 4 including Aguascalientes, Durango, Queretaro, and

756   Zacatecas shows a rising pattern in the growth rate (Figure 11). This information can be utilized

757   by the states in guiding their decision regarding the implementation of public health measures.

758   For example, states in cluster 1 and 4 may need strict public health measures to contain the

759   epidemic.

760

761   Appropriate short-term forecasts can also help gauge the impact of interventions in near real-

762   time. In this study we compared the performance of our three models for short-term real-time

763   forecasting the COVID-19 mortality estimates in Mexico and Mexico City. As in Figs 2-5 the

764   sub-epidemic model can be declared the most appropriate model as it exhibits the most desirable

765   performance metrics across majority of the calibration and forecasting phases. This model has

766   the capacity to accommodate more complex epidemic trajectories suggesting a longer epidemic

767   wave and can better adjust to the early signs of changes in disease transmission, while other

768   models (GLM and Richards) are less reactive. This model can also be utilized as a potential

769 forecasting tool for other cities in Mexico; comparing its results with other prediction models.

770 Moreover, further short-term forecasts (5,10 days) could be also be conducted with the sub-

771 epidemic model using the consecutive calibration phases to reduce the error metrics [52].

772

773 Overall, the sequential forecasts based on the daily smoothed death estimates for Mexico from

774 the two models (GLM, Richards) suggest a decline in over-all deaths (S1 Fig and S2 Fig)

775 consistent with the sustained decline in COVID-19 associated case fatalities since mid-August as

776 reported by the Mexican government, officially [99]. However, this decline in COVID-19 deaths

777 can be attributed to the inaccurate reporting of deaths in the surveillance system or downplay of

778 fatalities by the government. For instance, the reported excess deaths as of September 26, 2020

779 are estimated to be 193170, with 139151 deaths attributable to COVID-19 [100]. While the

780 official tally of COVID-19 deaths in Mexico is only exceeded by USA and Brazil, its roughly

781 approximated with that of India, a country whose population is ten times larger than Mexico

782 [101]. As observed earlier, the easing of the social distancing interventions and lifting of

783 lockdowns in Mexico in the month of June led to a surge of the COVID-19 associated deaths

784 [102]. In June, the government of Mexico also inaccurately forecasted that a potential decline in

785 the number of COVID-19 deaths will be observed by September, 2020 [103]. Therefore, the

786 forecasting trends need to be interpreted cautiously in order to inform policies. The IHME model

787 also shows a decline in COVID-19 deaths in Mexico from mid-August-September, which have

788 stabilized since then for the last six forecast periods (S5 Fig). The sub-epidemic model also

789 indicates a stabilization of the deaths for the last seven forecast periods (S6 Fig) consistent with

790 the results obtained from the IHME model.

791

792   Similarly, for Mexico City, the sequential forecasts obtained from the GLM and Richards model

793   fit to the daily death data estimates indicate a decline in the overall deaths (S3 Fig, S4 Fig). The

794   IHME and sub-epidemic models on the other hand indicate a stabilized trajectory of deaths for

795   the last three forecast periods (S7 Fig and S8 Fig) (suggesting that the actual death counts might

796   not be decreasing in Mexico City) as seen with Mexico. Based on the death data, the observed

797   decline or stability in death predictions could likely reflect the false slowing down of the

798   epidemic in Mexico City [102]. Moreover, insufficient testing can also result in an inaccurate

799   trajectory of the COVID-19 mortality curve [104].

800

801   The cumulative comparison of deaths in Mexico and Mexico City indicates that in general, the

802   Richards model has under-performed in predicting the actual death counts with much wider

803   uncertainty around the mean death estimates. The Richards model has also failed to capture the

804   early sub-exponential dynamics of the mortality curve. The cumulative death counts obtained

805   from the flexible sub-epidemic model closely approximate the total mean death counts obtained

806   from the three IHME modeling scenarios. Whereas the GLM slightly under predicts the

807   cumulative death counts (Fig 6, Fig 7). On the other hand, another competing model, the

808   COVID-19 predictions model projects 87,151 deaths (95% PI:84,414, 91,883) for Mexico as of

809   October 27, 2020 (last forecasting phase), an estimate that closely approximates the estimates

810   obtained from the GLM model (between 77,258-93,454 deaths) [105].

811

812   The three models (GLM, Richards, sub-epidemic model) used in this study generally provide

813   good fits to the mortality curve based on the residuals. The Richards model however is unable to

814   capture the early sub-exponential dynamics of the mortality curve. Moreover, these

815   phenomenological models are particularly valuable for providing rapid predictions of the

816   epidemics in complex scenarios that can be used for real-time preparedness since these models

817   do not require specific disease transmission processes to account for the interventions. Since

818   these models do not explicitly account for behavioral changes, the results should be interpreted

819   with caution. Importantly, since the mortality curves employed in this study are reported

820   according to the date of reporting, they are likely influenced by variation in the testing rates and

821   related factors including the case fatality rates. Further, delays in reporting of deaths due to the

822   magnitude of the epidemic could also influence our predictions. Moreover, using the reporting

823   date is not ideal due to the time difference between the date of death and the reporting date of

824   death, which at a given moment can give a false impression of the ongoing circumstances.

825

826   This paper is not exempt from limitations. First, the IHME (current projections, mandated mask,

827   and worst-case scenario) model utilized has been revised multiple times over the course of the

828   pandemic and differs substantially in methodology, assumptions, range of predictions and

829   quantities estimated. Second, the IHME has been irregular in publishing the downloadable

830   estimates online for some periods. Third, we model the death estimates by date of reporting

831   rather than by the date of death. Lastly, the unpredictable social component of the epidemic on

832   ground is also a limiting factor for the study as we do not know the ground truth mortality pattern

833   when the forecasts are generated.

834

835   In conclusion, the reproduction number has been fluctuating around ~1.0 since the end of July-

836   end of September 2020, indicating sustained virus transmission in the region. Moreover, the

837   country has seen much lower mobility reduction and mixed reactions towards the stay-at-home

838   orders contributing towards the virus transmission in the country. Moreover, the spatial analysis

839   indicates that states like Mexico, Michoacán, Morelos, Nuevo Leon, Baja California need to put

840   in place stronger public health strategies to contain the rising patterns in growth rates. The GLM

841   and sub-epidemic model applied to mortality data in Mexico provide reasonable estimates for

842   short-term projections in near real-time. While the GLM and Richards models predict that the

843   COVID-19 outbreak in Mexico and Mexico City may be on a sustained decline, the sub-

844   epidemic model and IHME model predict a stabilization of daily deaths. However, our forecasts

845   need to be interpreted with caution given the dynamic implementation and lifting of the social

846   distancing measures.

847

848   **Author Contributions**: Conceptualization, G.C. and A.T.; methodology, G.C, A.T.; validation,

849   G.C.; formal analysis, A.T., G.C.; investigation, A.T. S.D., J.M.B., P.S. ; resources, G.C., A.T.

850   J.M.B., B.E. A.B, P.S; data curation, A.T.; writing—original draft preparation, A.T., G.C.;

851   writing, review and editing, A.T., G.C., J.M.B., P.S., S.D., C.C.G, B.E., N.G.B., R.A.S, A.K,

852   R.L, A.S, H.G., N.G.C., A.I.B., M.E.J; visualization, A.T., G.C.; supervision, G.C.; project

853   administration, G.C.; funding acquisition, G.C. All authors have read and agreed to the published

854   version of the manuscript.

855

858

859   **Conflicts of Interest**: The authors declare no conflict of interest.

860
861   **References**

41

862   1.   Johnson NP, Mueller J. Updating the accounts: global mortality of the 1918-1920
863   "Spanish" influenza pandemic. Bull Hist Med. 2002;76(1):105-15.
864   2.   Cascella M, Rajnik M, Cuomo A, Dulebohn SC, Di Napoli R. Features, Evaluation, and
865   Treatment of Coronavirus (COVID-19). StatPearls. Treasure Island (FL): StatPearls Publishing
866   Copyright © 2020, StatPearls Publishing LLC.; 2020.
867   3.   Li Z, Chen Q, Feng L, Rodewald L, Xia Y, Yu H, et al. Active case finding with case
868   management: the key to tackling the COVID-19 pandemic. The Lancet. 2020;396(10243):63-70.
869   4.   COVID-19 coronavirus / cases [Internet]. 2020. Available from:
870   https://www.worldometers.info/coronavirus/coronavirus-cases/.
871   5.   WHO. Situation Reports Coronavirus World Health Organization2020 [Available from:
872   https://www.who.int/emergencies/diseases/novel-coronavirus-2019/situation-reports.
873   6.   WHO. Summary of probable SARS cases with onset of illness from 1 November 2002 to
874   31 July 2003 2003 [Available from:
875   https://www.who.int/csr/sars/country/table2004_04_21/en/.
876   7.   WHO. MERS situation update November 2019. World Health Organization; 2019.
877   8.   The L. COVID-19 vaccines: no time for complacency. The Lancet. 2020;396(10263):1607.
878   9.   Ledford H. US authorization of first COVID vaccine marks new phase in safety
879   monitoring. Nature. 2020.
880   10.   Reiner RC, Barber RM, Collins JK, Zheng P, Adolph C, Albright J, et al. Modeling COVID-19
881   scenarios for the United States. Nature Medicine. 2021;27(1):94-105.
882   11.   Azanza Ricardo CL, Hernandez Vargas EA. The Risk of Lifting COVID-19 Confinement in
883   Mexico. medRxiv. 2020:2020.05.28.20115063.
884   12.   Shuchman M. Low- and middle-income countries face up to COVID-19. Nature Medicine.
885   2020(26):986-8.
886   13.   Barnett-Howell Z, Mobarak AM. Should Low-Income Countries Impose the Same Social
887   Distancing Guidelines as Europe and North America to Halt the Spread of COVID-19? 2020
888   [cited 2020 April 2]. Available from: https://som.yale.edu/should-low-income-countries-
889   impose-the-same-social-distancing-guidelines-as-europe-and-north-america-to-halt-the-
890   spread-of-covid-19.
891   14.   Regmi K, Lwin CM. Impact of social distancing measures for preventing coronavirus
892   disease 2019 [COVID-19]: A systematic review and meta-analysis protocol. medRxiv.
893   2020:2020.06.13.20130294.
894   15.   MOH. Ministry of Health Mexico 2020 [Available from:
895   https://www.gob.mx/salud/documentos/datos-abiertos-152127.
896   16.   Statistica. Number of people living in poverty in Mexico between 2008 and 2018(in
897   millions) 2019 [cited 2019 July]. Available from:
898   https://www.statista.com/statistics/1039479/mexico-people-living-poverty/.
899   17.   Coneval. Poverty measurement, poverty measurement in Mexico 2020 [Available from:
900   https://www.coneval.org.mx/Medicion/Paginas/PobrezaInicio.aspx.
901   18.   Organization IL. Informal employment in Mexico: Current situation, policies and
902   challenges. 2014.
903   19.   Agren D. Understanding Mexican health worker COVID-19 deaths. The Lancet.
904   2020;396(10254):807.

905   20.   Montes J. Covid-19 Takes Outsize Toll on Mexican Health Workers. The Wall Street
906   Journal. 2021 January 9.
907   21.   Data OWi. Total COVID-19 tests per 1,000 people 2020 [Available from:
908   https://ourworldindata.org/grapher/full-list-cumulative-total-tests-per-thousand?time=2020-
909   02-21..latest&country=BRA~CHL~SLV~MEX~PER.
910   22.   Moreno T. Mexico's COVID-19 contingency plan: three key phases to fight the
911   coronavirus outbreak
912   . El Universal. 2020 March 14.
913   23.   Drafting. There are 3 confirmed cases of coronavirus in Mexico. Elfinanciero. February
914   28, 2020.
915   24.   Expansion P. The Ministry of Health confirms the sixth case of coronavirus in Mexico.
916   Political expansion. March 6, 2020.
917   25.   Informer T. Massive Activities Due to Coronavirus Suspended. InformadorMx. March
918   13, 2020.
919   26.   Taylor L. Covid-19: How denialism led Mexico's disastrous pandemic control effort. BMJ.
920   2020;371:m4952.
921   27.   Agren D. Mexico holds off canceling mass gatherings amid coronavirus threat. USA
922   Today. 2020 March 14.
923   28.   Caicedo-Ochoa Y, Rebellón-Sánchez DE, Peñaloza-Rallón M, Cortés-Motta HF, Méndez-
924   Fandiño YR. Effective Reproductive Number estimation for initial stage of COVID-19 pandemic
925   in Latin American Countries. International Journal of Infectious Diseases. 2020;95:316-8.
926   29.   Ibarra-Nava I, Cardenas-de la Garza JA, Ruiz-Lozano RE, Salazar-Montalvo RG. Mexico
927   and the COVID-19 Response. Disaster Medicine and Public Health Preparedness.
928   2020;14(4):e17-e8.
929   30.   Suárez V, Suarez Quezada M, Oros Ruiz S, Ronquillo De Jesús E. Epidemiology of COVID-
930   19 in Mexico: From the 27th of February to the 30th of April 2020. Rev Clin Esp (Barc).
931   2020;220(8):463-71.
932   31.   GardaWorld. Mexico: Government enters phase 2 of COVID-19 contingency plan on
933   March 24 /update 3. GradaWorld. 2020 March 28.
934   32.   GardaWorld. Mexico: Authorities declare health emergency as COVID-19 cases exceed
935   1000 March 30 /update 4. GardaWorld. 2020 March 31.
936   33.   Fredrick J. 'If Coronavirus Doesn't Kill Me, Hunger Will': Mexico's Poor Bear Brunt Of
937   Pandemic. Npr. 2020 July 30.
938   34.   Blust K. Sonoran authorities will enforce strict stay-at-home order through April 30.
939   News Azpm. 2020 April 13.
940   35.   Secretaría de Gobernación DOdIF. cuerdo por el que se establecen las medidas
941   preventivas que se deberán implementar para la mitigación y control de los riesgos para la
942   salud que implica la enfermedad por el virus SARS-CoV2 (COVID-19). 2020 March 24.
943   36.   Wall SAA. Be okay with the "stay home". Psico Grupo; 2020 May 21.
944   37.   AP. Mexico to restrict mobility to areas less affected by virus. AP News. April 16, 2020.
945   38.   Universal E. Mexico enters Phase 3 of its contingency plan to fight COVID-19. El
946   Universal. 2020 April 4.

947   39.   Capistran MA, Capella A, Christen JA. Forecasting hospital demand in metropolitan areas
948   during the current COVID-19 pandemic and estimates of lockdown-induced 2nd waves.
949   medRxiv. 2020:2020.07.16.20155721.
950   40.   Oré D. Exclusive: 'We're winning' - Mexico's coronavirus czar sees victory in sight.
951   Reuters. 2020 May 5.
952   41.   Ahmed A, Kurmanaev A, Politi D, Londoño E. Virus Gains Steam Across Latin America.
953   NewYork Times. 2020 June 23.
954   42.   Flores J. Did the mathematical model fail? Nexos: Nexos; 2020 [updated July 9. Available
955   from: https://datos.nexos.com.mx/?p=1485.
956   43.   Press A. Mexico President Kicks off 'New Normal' Phase Amid Pandemic. US News. 2020
957   June 1.
958   44.   Review TNL. Red, Orange, Yellow, Green—Go! Considerations for Reopening in Mexico:
959   Social, Educational, and Economic Activities. The National Law Review. 2020 June 16.
960   45.   Deakins O. Mexico's COVID-19 Traffic Light Monitoring System: News for August 17–30,
961   2020. Ogletree Deakins. 2020 August 21.
962   46.   Chowell G, Hincapie-Palacio D, Ospina J, Pell B, Tariq A, Dahal S, et al. Using
963   Phenomenological Models to Characterize Transmissibility and Forecast Patterns and Final
964   Burden of Zika Epidemics. Public Library of Science Currents.
965   2016;8:ecurrents.outbreaks.f14b2217c902f453d9320a43a35b583.
966   47.   Pell B, Kuang Y, Viboud C, Chowell G. Using phenomenological models for forecasting
967   the 2015 Ebola challenge. Epidemics. 2018;22:62-70.
968   48.   IHME. COVID-19 Projections 2020 [updated June 10. Available from:
969   https://covid19.healthdata.org/mexico.
970   49.   Apple. Mobility Trends Reports Apple 2020 [cited 2020. Available from:
971   https://covid19.apple.com/mobility.
972   50.   Shu Y, McCauley J. GISAID: Global initiative on sharing all influenza data - from vision to
973   reality. Euro surveillance : bulletin Europeen sur les maladies transmissibles = European
974   communicable disease bulletin. 2017;22(13):30494.
975   51.   Banda JM, Tekumalla R, Wang G, Yu J, Liu T, Ding Y, et al. A large-scale COVID-19 Twitter
976   chatter dataset for open scientific research -- an international collaboration. ArXiv. 2020.
977   52.   Chowell G, Tariq A, Hyman JM. A novel sub-epidemic modeling framework for short-
978   term forecasting epidemic waves. BioMed Central Medicine. 2019;17(1):164.
979   53.   Shanafelt DW, Jones G, Lima M, Perrings C, Chowell G. Forecasting the 2001 Foot-and-
980   Mouth Disease Epidemic in the UK. Ecohealth. 2018;15(2):338-47.
981   54.   Roosa K, Lee Y, Luo R, Kirpich A, Rothenberg R, Hyman JM, et al. Short-term Forecasts of
982   the COVID-19 Epidemic in Guangdong and Zhejiang, China: February 13-23, 2020. Journal of
983   clinical medicine. 2020;9(2):596.
984   55.   Roosa K, Lee Y, Luo R, Kirpich A, Rothenberg R, Hyman JM, et al. Real-time forecasts of
985   the COVID-19 epidemic in China from February 5th to February 24th, 2020. Infectious Disease
986   Modelling. 2020;5:256-63.
987   56.   Richards FJ. A Flexible Growth Function for Empirical Use. Journal of Experimental
988   Botany. 1959;10(2):290-301.
989   57.   Banks HT, Hu S, Thompson WC. Modeling and inverse problems in the presence of
990   uncertainty: CRC Press; 2014.

991   58.   Chowell G. Fitting dynamic models to epidemic outbreaks with quantified uncertainty: A
992   primer for parameter uncertainty, identifiability, and forecasts. Infectious Disease Modelling.
993   2017;2(3):379-98.
994   59.   Mathworks. lhs design [Available from:
995   https://www.mathworks.com/help/stats/lhsdesign.html.
996   60.   Roosa K, Luo R, Gerardo C. Comparative assessment of parameter estimation methods
997   in the presence of overdispersion: a simulation study. Mathematical Biosciences and
998   Engineering. 2019;16(5):4299-313.
999   61.   Roosa K, Chowell G. Assessing parameter identifiability in compartmental dynamic
1000   models using a computational approach: application to infectious disease transmission models.
1001   Theoretical Biology and Medical Modelling. 2019;16(1):1.
1002   62.   M K, K. J. Applied predictive modeling. New York: Springer; 2013.
1003   63.   Gneiting T, Raftery AE. Strictly Proper Scoring Rules, Prediction, and Estimation. Journal
1004   of the American Statistical Association. 2007;102(477):359-78.
1005   64.   Healy K. Apple's COVID Mobility Data. Github: Github; 2020.
1006   65.   Chowell G, Abdirizak F, Lee S, Lee J, Jung E, Nishiura H, et al. Transmission characteristics
1007   of MERS and SARS in the healthcare setting: a comparative study. BioMed Central Medicine.
1008   2015;13(1):210.
1009   66.   Anderson RM, May RM. Infectious Diseases of Humans. Oxford, editor. Oxford
1010   Univeristy Press1991.
1011   67.   Nishiura H, Chowell G, Heesterbeek H, Wallinga J. The ideal reporting interval for an
1012   epidemic to objectively interpret the epidemiological time course. J R Soc Interface.
1013   2010;7(43):297-307.
1014   68.   Viboud C, Simonsen L, Chowell G. A generalized-growth model to characterize the early
1015   ascending phase of infectious disease outbreaks. Epidemics. 2016;15:27-37.
1016   69.   Ganyani T, Kremer C, Chen D, Torneri A, Faes C, Wallinga J, et al. Estimating the
1017   generation interval for coronavirus disease (COVID-19) based on symptom onset data, March
1018   2020. Eurosurveillance. 2020;25(17):2000257.
1019   70.   Nishiura H, Chowell G. Early transmission dynamics of Ebola virus disease (EVD), West
1020   Africa, March to August 2014. Euro surveillance : bulletin Europeen sur les maladies
1021   transmissibles = European communicable disease bulletin. 2014;19(36).
1022   71.   H. Nishiura GC. The Effective Reproduction Number as a Prelude to Statistical Estimation
1023   of Time-Dependent Epidemic Trends. Springer D, editor2009. 103-12 p.
1024   72.   Paine S, Mercer G, Kelly P, Bandaranayake D, Baker M, Huang Q, et al. Transmissibility of
1025   2009 pandemic influenza A(H1N1) in New Zealand: effective reproduction number and
1026   influence of age, ethnicity and importations. Euro surveillance : bulletin Europeen sur les
1027   maladies transmissibles = European communicable disease bulletin. 2010;15(24).
1028   73.   Fraser C. Estimating Individual and Household Reproduction Numbers in an Emerging
1029   Epidemic. PLOS ONE. 2007;2(8):e758.
1030   74.   Chong KC, Zee BCY, Wang MH. Approximate Bayesian algorithm to estimate the basic
1031   reproduction number in an influenza pandemic using arrival times of imported cases. Travel
1032   medicine and infectious disease. 2018;23:80-6.
1033   75.   He X, Lau EHY, Wu P, Deng X, Wang J, Hao X, et al. Temporal dynamics in viral shedding
1034   and transmissibility of COVID-19. Nature Medicine. 2020;26(5):672-5.

1035   76.   Wallinga J, Teunis P. Different Epidemic Curves for Severe Acute Respiratory Syndrome
1036   Reveal Similar Impacts of Control Measures. American Journal of Epidemiology.
1037   2004;160(6):509-16.
1038   77.   Cori A, Ferguson NM, Fraser C, Cauchemez S. A New Framework and Software to
1039   Estimate Time-Varying Reproduction Numbers During Epidemics. American Journal of
1040   Epidemiology. 2013;178(9):1505-12.
1041   78.   Wu F, Zhao S, Yu B, Chen Y-M, Wang W, Hu Y, et al. Complete genome characterisation
1042   of a novel coronavirus associated with severe human respiratory disease in Wuhan, China.
1043   bioRxiv. 2020:2020.01.24.919183.
1044   79.   Edgar RC. MUSCLE: multiple sequence alignment with high accuracy and high
1045   throughput. Nucleic Acids Res. 2004;32(5):1792-7.
1046   80.   Stamatakis A. RAxML version 8: a tool for phylogenetic analysis and post-analysis of
1047   large phylogenies. Bioinformatics. 2014;30(9):1312-3.
1048   81.   Suchard MA, Lemey P, Baele G, Ayres DL, Drummond AJ, Rambaut A. Bayesian
1049   phylogenetic and phylodynamic data integration using BEAST 1.10. Virus Evol.
1050   2018;4(1):vey016.
1051   82.   Li Q, Guan X, Wu P, Wang X, Zhou L, Tong Y, et al. Early Transmission Dynamics in
1052   Wuhan, China, of Novel Coronavirus–Infected Pneumonia. New England Journal of Medicine.
1053   2020.
1054   83.   Srivastava A, Chowell G. Understanding Spatial Heterogeneity of COVID-19 Pandemic
1055   Using Shape Analysis of Growth Rate Curves. Preprint medRxiv. 2020:2020.05.25.20112433.
1056   84.   Srivastava A, Chowell G. Understanding Spatial Heterogeneity of COVID-19 Pandemic
1057   Using Shape Analysis of Growth Rate Curves. medRxiv.
1058   85.   Srivastava A, Klassen EP. Functional and shape data analysis: Springer; 2016.
1059   86.   Alliance DP. C-19 Global South obervatory Mexico 2020 [Available from:
1060   https://datapopalliance.org/covid19/c19globalsouthobservatory/mexico/.
1061   87.   Chowell G, Viboud C, Hyman JM, Simonsen L. The Western Africa ebola virus disease
1062   epidemic exhibits both global exponential and local polynomial growth rates. PLoS currents.
1063   2015;7.
1064   88.   Mendoza CI. Inhomogeneous mixing and asynchronic transmission between local
1065   outbreaks account for the spread of COVID-19 epidemics. medRxiv. 2020:2020.08.04.20168443.
1066   89.   Tariq A, Undurraga EA, Laborde CC, Vogt-Geisse K, Luo R, Rothenberg R, et al. Early
1067   transmission dynamics of COVID-19 in Chile: From sub-exponential ascending growth dynamics
1068   to a stationary disease wave, March-April, 2020. medRxiv. 2020:2020.05.15.20103069.
1069   90.   Anzarut M, González LF, Mendizábal S, Ortiz MT. Estimating COVID-19 cases and
1070   reproduction number in Mexico. Arxiv. 2020.
1071   91.   Canals M, Cuadrado C, Canals A, Yohannessen K, Lefio LA, Bertoglia MP, et al. Epidemic
1072   trends, public health response and health system capacity: the Chilean experience in four
1073   months of the COVID-19 pandemic. Rev Panam Salud Publica. 2020;44:e99-e.
1074   92.   Tariq A, Undurraga EA, Laborde CC, Vogt-Geisse K, Luo R, Rothenberg R, et al.
1075   Transmission dynamics and control of COVID-19 in Chile, March-October, 2020. medRxiv : the
1076   preprint server for health sciences. 2020:2020.05.15.20103069.

1077   93.   Munayco CV, Tariq A, Rothenberg R, Soto-Cabezas GG, Reyes MF, Valle A, et al. Early
1078   transmission dynamics of COVID-19 in a southern hemisphere setting: Lima-Peru: February
1079   29th–March 30th, 2020. Infectious Disease Modelling. 2020;5:338-45.
1080   94.   Felix FHC, Fontenele JB. Instantaneous R calculation for COVID-19 epidemic in Brazil.
1081   medRxiv. 2020:2020.04.23.20077172.
1082   95.   Acuña-Zegarra MA, Santana-Cibrian M, Velasco-Hernandez JX. Modeling behavioral
1083   change and COVID-19 containment in Mexico: A trade-off between lockdown and compliance.
1084   Math Biosci. 2020;325:108370-.
1085   96.   Lopez O. Tourists Are Returning to Cancún. But Workers' Fears About COVID-19 Never
1086   Went Away. Time. 2021 January 11.
1087   97.   Kitroeff N. Mexico Misled Citizens About the Severity of Coronavirus in its Capital. The
1088   Newyork Times. 2020 December 21.
1089   98.   News T. Mexico, the Latin American country that least respects "stay at home": mobility
1090   report. Televisa News. 2020 April 7.
1091   99.   Rueters T. Mexico officials says coronavirus cases are on a 'sustained decline'. Rueters.
1092   2020 August 19.
1093   100.   AP. Mexico reported 193,170 "excess deaths" through Sept 26. AP. 2020 October 25.
1094   101.   Flannery NP. Why Are So Many People Dying Of Covid-19 In Mexico? Forbes. 2020
1095   September 3.
1096   102.   Mahase E. Covid-19: Deaths in Mexico triple since reopening began in June. BMJ.
1097   2020;370:m2753.
1098   103.   Daily MN. Covid deaths to stabilize in September, says Mexico City health minister.
1099   Mexico News Daily. 2020 September 30.
1100   104.   News B. Coronavirus: Mexico's death toll passes 30,000. BBC News. 2020 July 5.
1101   105.   Gu Y. COVID-19 Projections Using Machine Learning 2020 [Available from:
1102   https://covid19-projections.com/mexico.
1103
1104
1105

1106

1107

1108

1109

1110

1111

1112

1113

1114

1115

1116

1117

1118

1119

1120 **Supporting Information**

1121 S1 Fig: COVID-19 deaths forecasts using daily deaths, GLM model, Mexico: 30-days ahead

1122 forecasts based on the Generalized Logistic Growth Model (GLM) calibrated using an increasing

1123 amount of daily death data (blue circles): 107, 114, 120, 128, 136, 151, 156, 164, 172, 179, 185,

1124 193, 193 epidemic days. The vertical dashed line indicates the end of the calibration period and

1125 start of the forecasting period. The mean (solid red line) and 95% PIs (dashed red lines) of the

1126 model fit and forecast are shown.

1127 S2 Fig: COVID-19 death forecasts using daily deaths, Richards model, Mexico: 30-days ahead

1128 forecasts based on the Richards model calibrated using an increasing amount of daily death data

1129 (blue circles): 107, 114, 120, 128, 136, 151, 156, 164, 172, 179, 185, 193, 193 epidemic days.

1130 The vertical dashed line indicates the end of the calibration period and start of the forecasting

1131 period. The mean (solid red line) and 95% PIs (dashed red lines) of the model fit and forecast are

1132 shown

1133 S3 Fig: COVID-19 death forecasts using daily deaths, GLM model, Mexico City: 30-days ahead

1134 forecasts based on the GLM model calibrated using an increasing amount of daily death data

1135 (blue circles): 107, 114, 120, 128, 136, 151, 156, 164, 172, 179, 185, 193, 193 epidemic days.

1136 The vertical dashed line indicates the end of the calibration period and start of the forecasting

48

1137   period. The mean (solid red line) and 95% PIs (dashed red lines) of the model fit and forecast are

1138   shown.

1139   S4 Fig: COVID-19 death forecasts using daily deaths, Richards model, Mexico City: 30-days

1140   ahead forecasts based on the Richards model calibrated using an increasing amount of daily

1141   death data (blue circles): 107, 114, 120, 128, 136, 151, 156, 164, 172, 179, 185, 193, 193

1142   epidemic days. The vertical dashed line indicates the end of the calibration period and start of the

1143   forecasting period. The mean (solid red line) and 95% PIs (dashed red lines) of the model fit and

1144   forecast are shown.

1145   S5 Fig: COVID-19 death forecasts using daily deaths, IHME model, Mexico: 30-days ahead

1146   forecasts based on the IHME model calibrated using an increasing amount of daily death data

1147   (blue circles): 107, 114, 120, 128, 136, 151, 156, 164, 172, 179, 185, 193, 193 epidemic days.

1148   The vertical dashed line indicates the end of the calibration period and start of the forecasting

1149   period. The mean (solid red line) and 95% PIs (dashed red lines) of the model fit and forecast are

1150   shown.

1151   S6 Fig: COVID-19 death forecasts using daily deaths, sub-epidemic wave model, Mexico: 30-

1152   days ahead forecasts based on the sub-epidemic wave model calibrated using an increasing

1153   amount of daily death data (blue circles): 107, 114, 120, 128, 136, 151, 156, 164, 172, 179, 185,

1154   193, 193 epidemic days. The vertical dashed line indicates the end of the calibration period and

1155   start of the forecasting period. The mean (solid red line) and 95% PIs (dashed red lines) of the

1156   model fit and forecast are shown.

1157   S7 Fig: COVID-19 death forecasts using daily deaths, IHME model, Mexico City: 30-days ahead

1158   forecasts based on the IHME model calibrated using an increasing amount of daily death data

1159   (blue circles): 107, 114, 120, 128, 136, 151, 156, 164, 172, 179, 185, 193, 193 epidemic days.

1160   The vertical dashed line indicates the end of the calibration period and start of the forecasting

1161   period. The mean (solid red line) and 95% PIs (dashed red lines) of the model fit and forecast are

1162   shown.

1163   S8 Fig: COVID-19 death forecasts using daily deaths, sub-epidemic wave model, Mexico City:

1164   30-days ahead forecasts based on the sub-epidemic wave model calibrated using an increasing

1165   amount of daily death data (blue circles): 107, 114, 120, 128, 136, 151, 156, 164, 172, 179, 185,

1166   193, 193 epidemic days. The vertical dashed line indicates the end of the calibration period and

1167   start of the forecasting period. The mean (solid red line) and 95% PIs (dashed red lines) of the

1168   model fit and forecast are shown.

1169   S9 Fig: COVID-19 deaths forecasts using cumulative deaths, GLM model, Mexico: 30-days

1170   ahead forecasts based on the Generalized Logistic Growth Model (GLM) calibrated using an

1171   increasing amount of cumulative death data (blue circles). The vertical dashed line indicates the

1172   end of the calibration period and start of the forecasting period. The mean (solid red line) and

1173   95% PIs (dashed red lines) of the model fit and forecast are shown.

1174   S10 Fig: COVID-19 death forecasts using cumulative deaths, IHME model, Mexico: 30-day

1175   ahead forecasts based on the IHME model calibrated using cumulative death data (blue circles).

1176   The vertical dashed line indicates the end of the calibration period and start of the forecasting

1177   period. The mean (solid red line) and 95% PIs (dashed red lines) of the model fit and forecast are

1178   shown.

1179   S11 Fig: COVID-19 death forecasts using cumulative deaths, Richards model, Mexico: 30-day

1180   ahead forecasts based on the Richards model calibrated using cumulative death data (blue

1181   circles). The vertical dashed line indicates the end of the calibration period and start of the

1182   forecasting period. The mean (solid red line) and 95% PIs (dashed red lines) of the model fit and

1183   forecast are shown.

1184   S12 Fig: COVID-19 death forecasts using cumulative deaths, sub-epidemic wave model,

1185   Mexico: 30-day ahead forecasts based on the Sub-epidemic wave model calibrated using

1186   cumulative death data (blue circles). The vertical dashed line indicates the end of the calibration

1187   period and start of the forecasting period. The mean (solid red line) and 95% PIs (dashed red

1188   lines) of the model fit and forecast are shown.

1189   S13 Fig: COVID-19 deaths forecasts using cumulative deaths, GLM model, Mexico City: 30-

1190   ahead forecasts based on the Generalized Logistic Growth Model (GLM) calibrated using

1191   cumulative death data (blue circles). The vertical dashed line indicates the end of the calibration

1192   period and start of the forecasting period. The mean (solid red line) and 95% PIs (dashed red

1193   lines) of the model fit and forecast are shown.

1194   S14 Fig: COVID-19 death forecasts using cumulative deaths, IHME model, Mexico City: 30-day

1195   ahead forecasts based on the IHME model calibrated using cumulative death data (blue circles).

1196   The vertical dashed line indicates the end of the calibration period and start of the forecasting

1197   period. The mean (solid red line) and 95% PIs (dashed red lines) of the model fit and forecast are

1198   shown.

1199   S15 Fig: COVID-19 death forecasts using cumulative deaths, Richards model, Mexico City: 30-

1200   day ahead forecasts based on the Richards model calibrated using cumulative death data (blue

1201   circles). The vertical dashed line indicates the end of the calibration period and start of the

1202   forecasting period. The mean (solid red line) and 95% PIs (dashed red lines) of the model fit and

1203   forecast are shown.

1204   S16 Fig: COVID-19 death forecasts using cumulative deaths, sub-epidemic wave model, Mexico

1205   City: 30-day ahead forecasts based on the Sub-epidemic wave model calibrated using cumulative

1206   death data (blue circles). The vertical dashed line indicates the end of the calibration period and

1207   start of the forecasting period. The mean (solid red line) and 95% PIs (dashed red lines) of the

1208   model fit and forecast are shown.

1209   S17 Fig: Pre-processing COVID-19 data into incidence rate functions. From left to right: original

1210   lab-confirmed COVID-19 cases, curve of daily new cases, smoothed and scaled rate curves,

1211   average of rate curves before scaling and smothing.

1212   S18 Fig: Clustering of states according to the shapes of their rate curves. The largest cluster –

1213   Cluster 1 – is shown in green while the smallest cluster – Cluster 3 – is shown in the black. One

1214   can see that states with similar shapes of rates curves are geographically close to each other.

1215   S19 Fig: Average shapes of the COVID-19 incidence rate curves, along with a one standard-

1216   deviation band around the average, in each of the clusters.

1217   S20 Fig: Cluster averages and overall average. These averages represent the four dominant

1218   patterns of incidence rates observed across all states.

1219   S21 Fig: Total number of COVID-19 cases as of December 5, 2020

1220   S22: COVID-19 epi-curve overlaid by the curve of stay-at-home orders tweets. Blue line

1221   indicates the number of cases by dates of onset and the orange line indicates the number of

1222   tweets referring to the stay-at-home orders.

1223

1224

1225

1226

1227

1228

1229

1230

1231

1232

1233

1234

1235

1236

1237
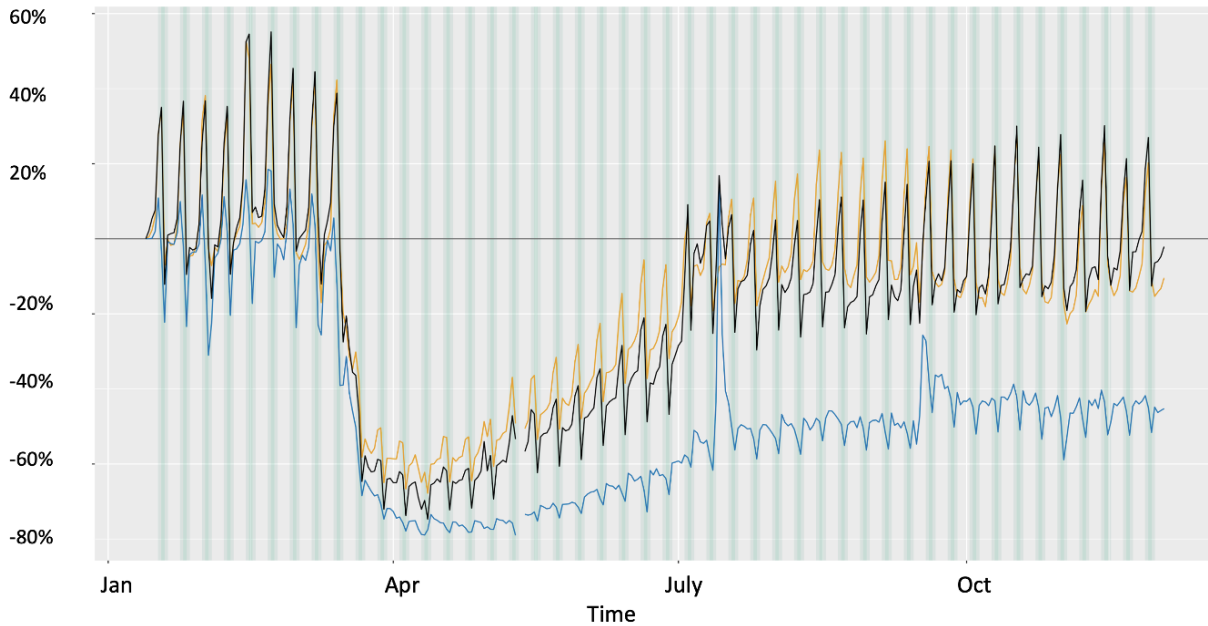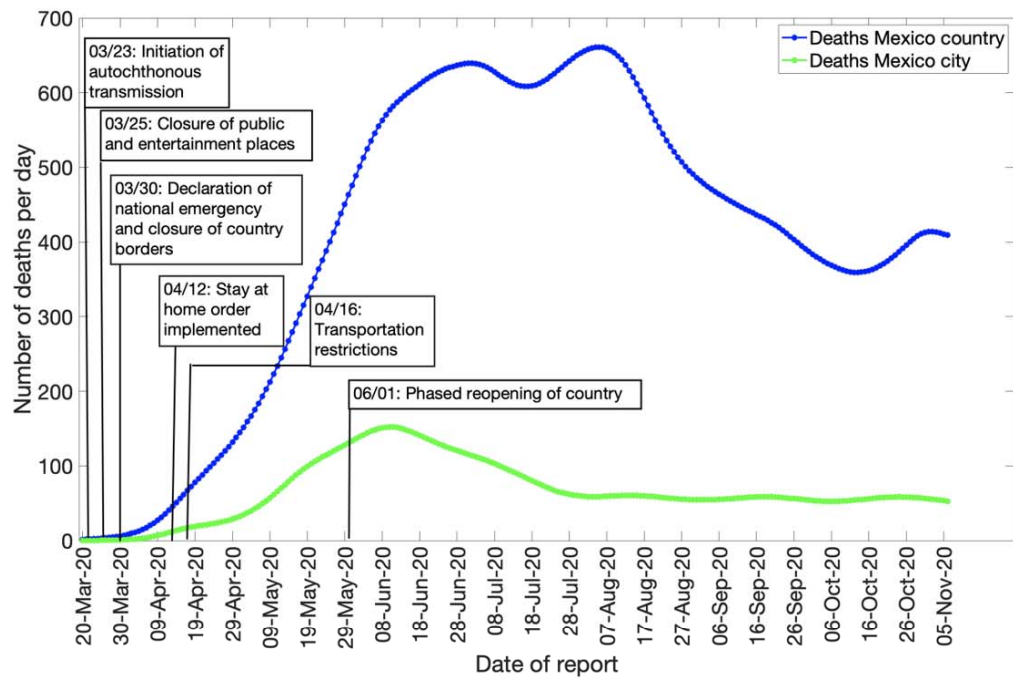
Fig 1: Upper panel: Epidemic curve for the COVID-19 deaths in Mexico and Mexico City from

March 20-November 11, 2020. Blue line depicts the confirmed deaths in Mexico and green line

depicts the confirmed deaths in Mexico City.

Lower panel: The mobility trends for Mexico. Orange line shows the driving trend, blue line

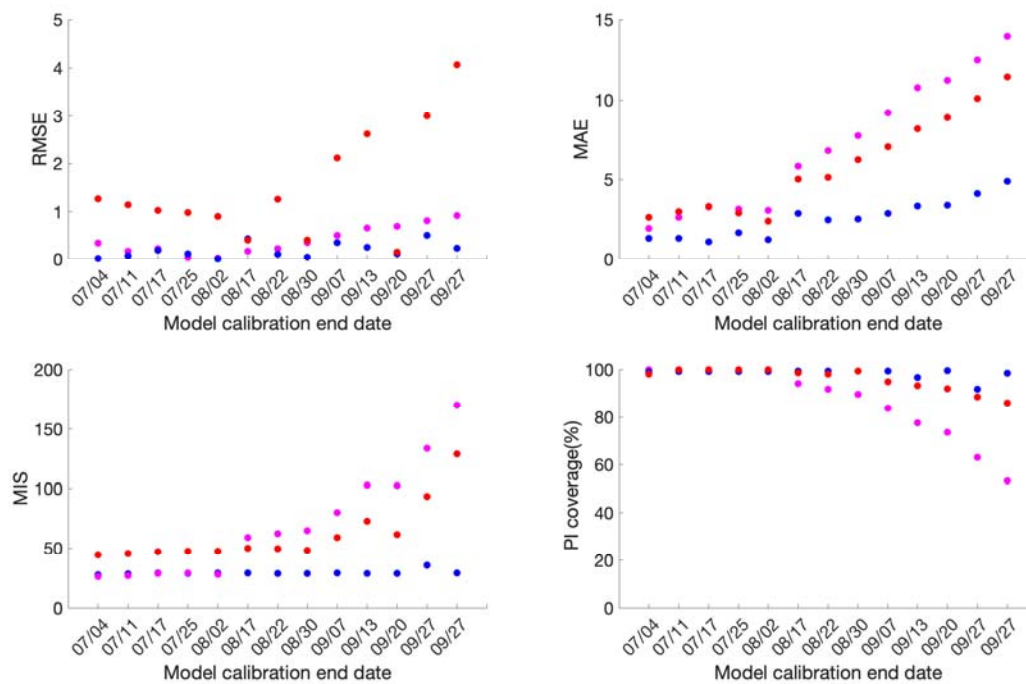shows the transit trend and the black line shows the walking trend.

54

1244

1245

Fig 2: Calibration performance for each of the thirteen sequential calibration phases for GLM (magenta), Richards (red) and sub-epidemic (blue) model for Mexico. High 95% PI coverage and lower mean interval score (MIS), root mean square error (RMSE) and mean absolute error (MAE) indicate better performance.

1250

1251

Fig 3: Calibration performance for each of the thirteen sequential calibration phases for GLM (magenta), Richards (red) and sub-epidemic (blue) model for Mexico City. High 95% PI coverage and lower mean interval score (MIS), root mean square error (RMSE) and mean absolute error (MAE) indicate better performance.

1256
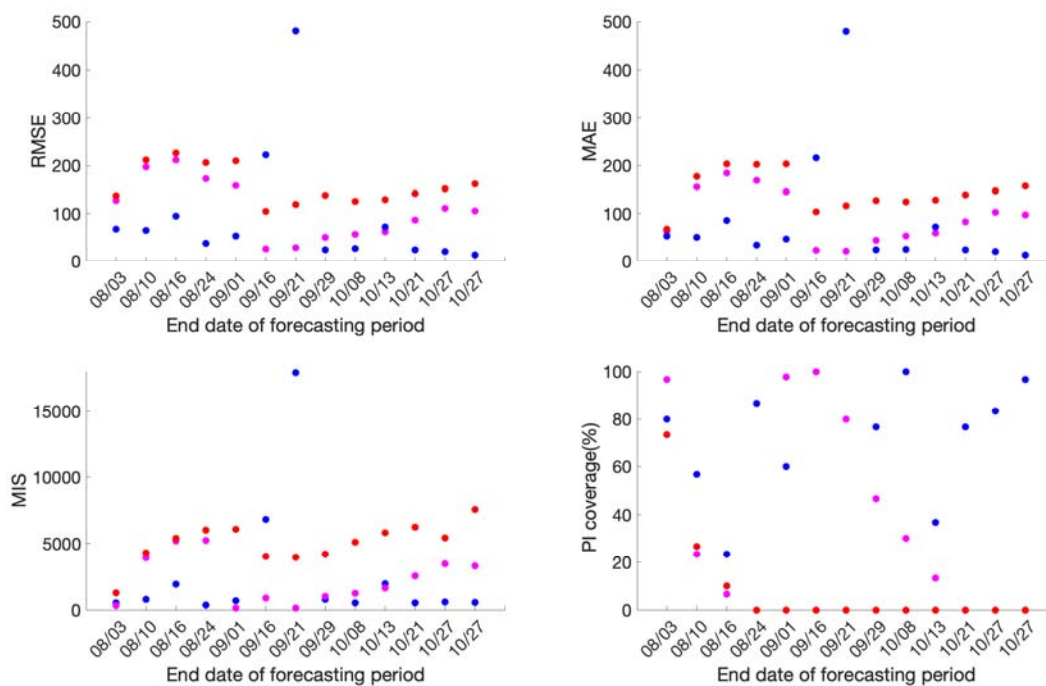
1257

1258

1259   Fig 4: Forecasting period performance metrics for each of the thirteen sequential forecasting

1260   phases for GLM (magenta), Richards (red) and sub-epidemic (blue) model for Mexico. High

1261   95% PI coverage and lower mean interval score (MIS), root mean square error (RMSE) and

1262   mean absolute error (MAE) indicate better performance.

1263
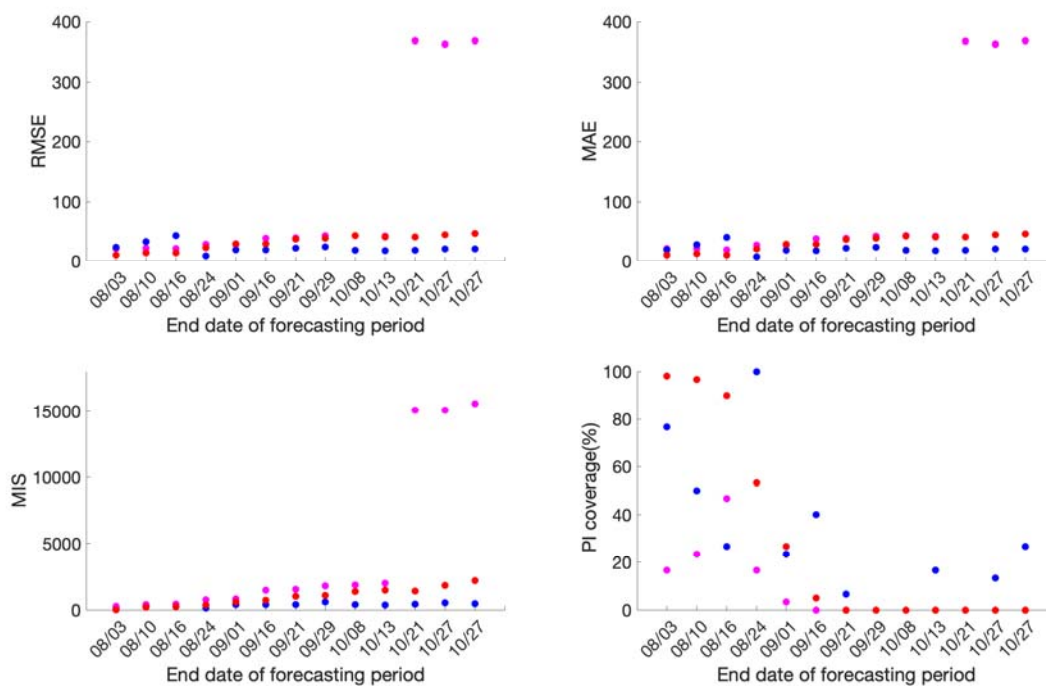
1264

1265

1266 Fig 5: Forecasting period performance metrics for each of the thirteen sequential forecasting

1267 phases for GLM (magenta), Richards (red) and sub-epidemic (blue) model for the Mexico City.

1268 High 95% PI coverage and lower mean interval score (MIS), root mean square error (RMSE) and

1269 mean absolute error (MAE) indicate better performance.

1270

1271

1272

1273

1274

1275

1276

1277
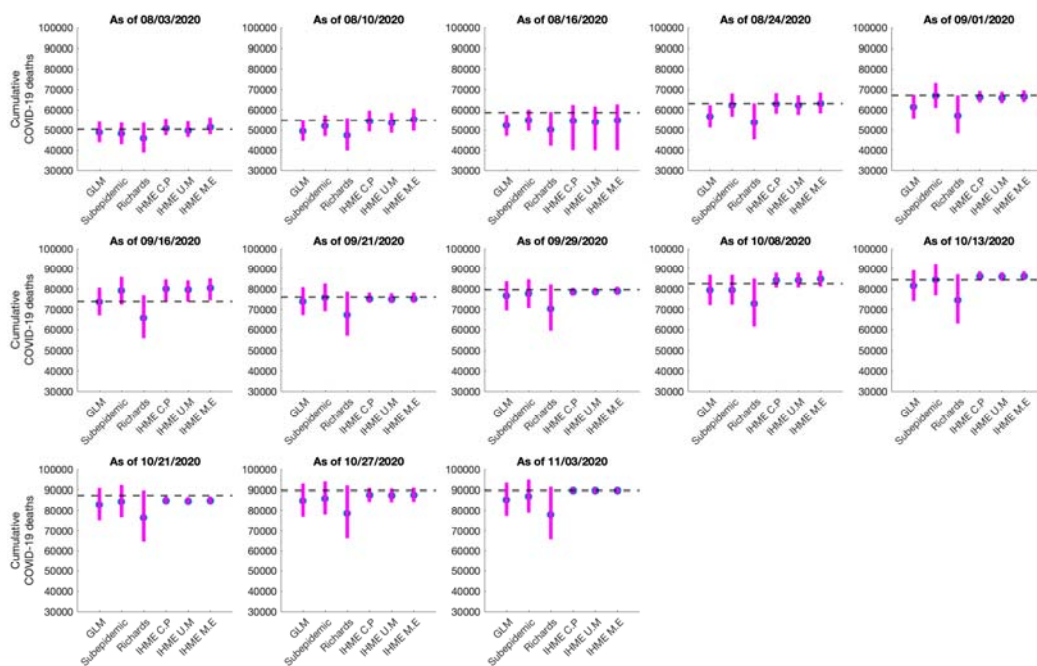
1278

1279

1280 Fig 6: Systematic comparison of the six models (GLM, Richards, sub-epidemic model, IHME

1281 current projections (IHME C.P), IHME universal masks (IHME U.M) and IHME mandates

1282 easing (IHME M.E)) to predict the cumulative COVID-19 deaths for Mexico in the thirteen

1283 sequential forecasts. The blue circles represent the mean deaths and the magenta vertical line

1284 indicates the 95% PI around the mean death count. The horizontal dashed line represents the

1285 actual death count reported by that date in the November 11, 2020 IHME estimates files.

1286

1287

1288

1289 5

1290

1291

1292
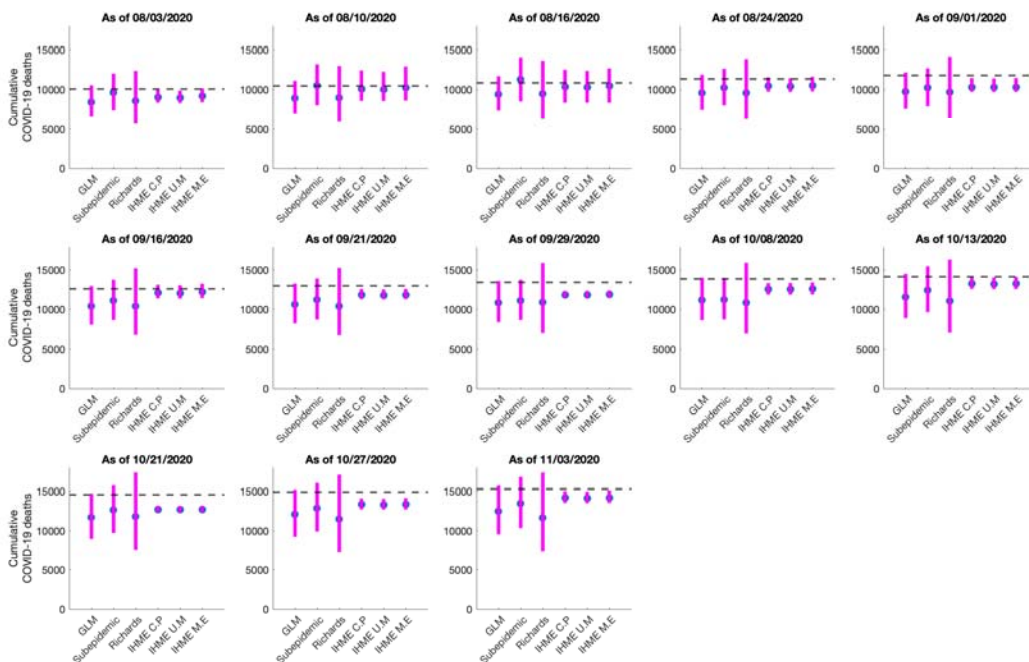
1293

Fig 7: Systematic comparison of the six (GLM, Richards, sub-epidemic model, IHME current projections (IHME C.P), IHME universal masks (IHME U.M) and IHME mandates easing (IHME M.E))to predict the cumulative COVID-19 deaths for the Mexico City in the thirteen sequential forecasts. The blue circles represent the mean deaths and the magenta vertical line indicates the 95% PI around the mean death count. The horizontal dashed line represents the actual death count reported by that date in the November 11, 2020 IHME estimates files.

1300

1301

1302

1303

1304

1305
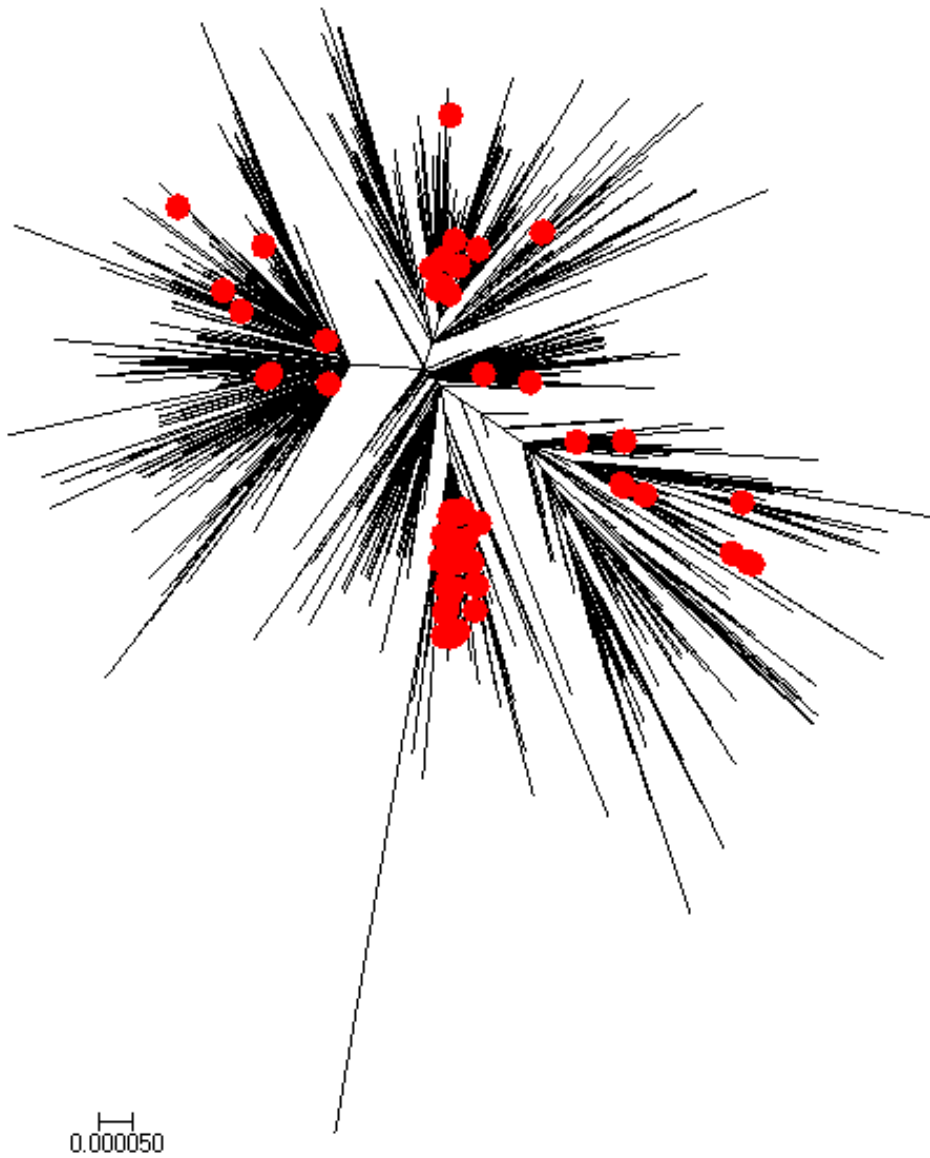
0.000050

1306

1307

1308

1309

1310   Fig 8: Global neighbor-joining tree for SARS-CoV-2 genomic data from February 27- May 29,

1311   2020 . Sequences sampled in Mexico are highlighted in red.
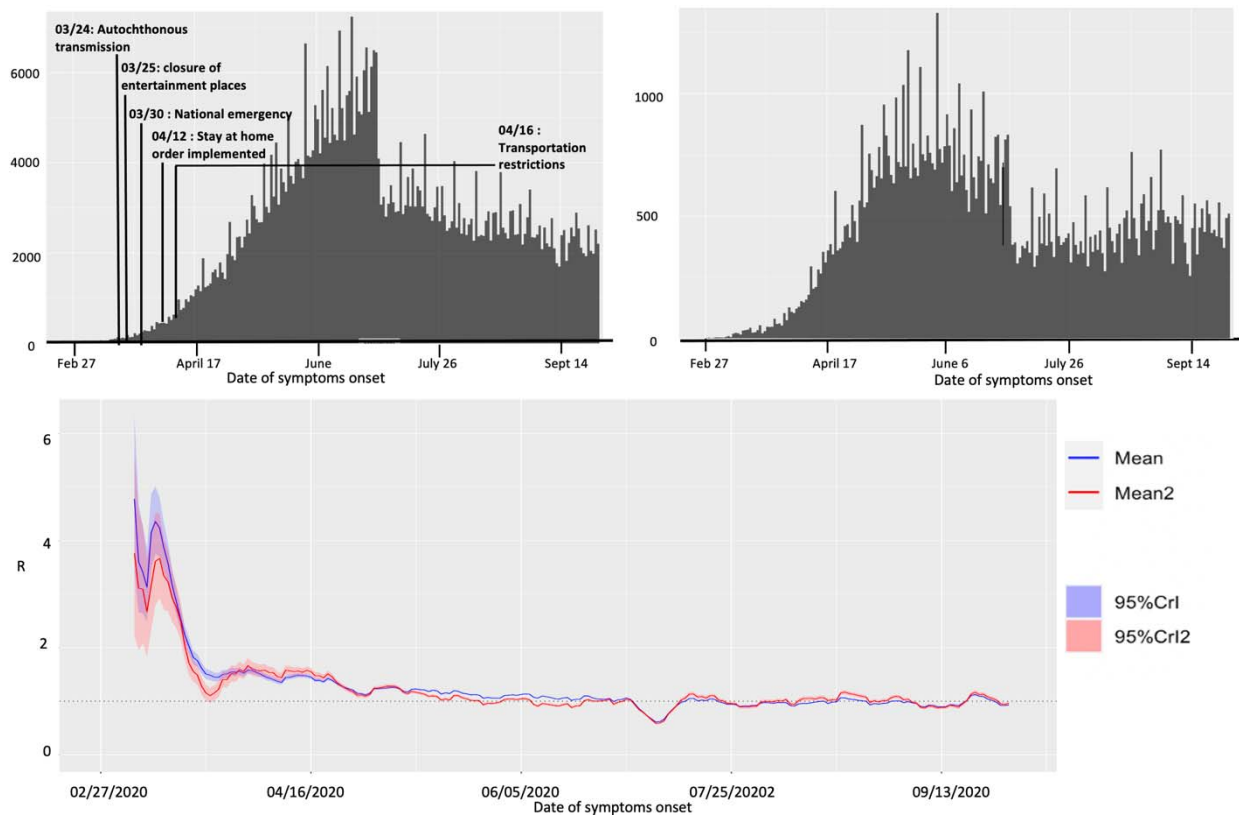
1312

1313

1314
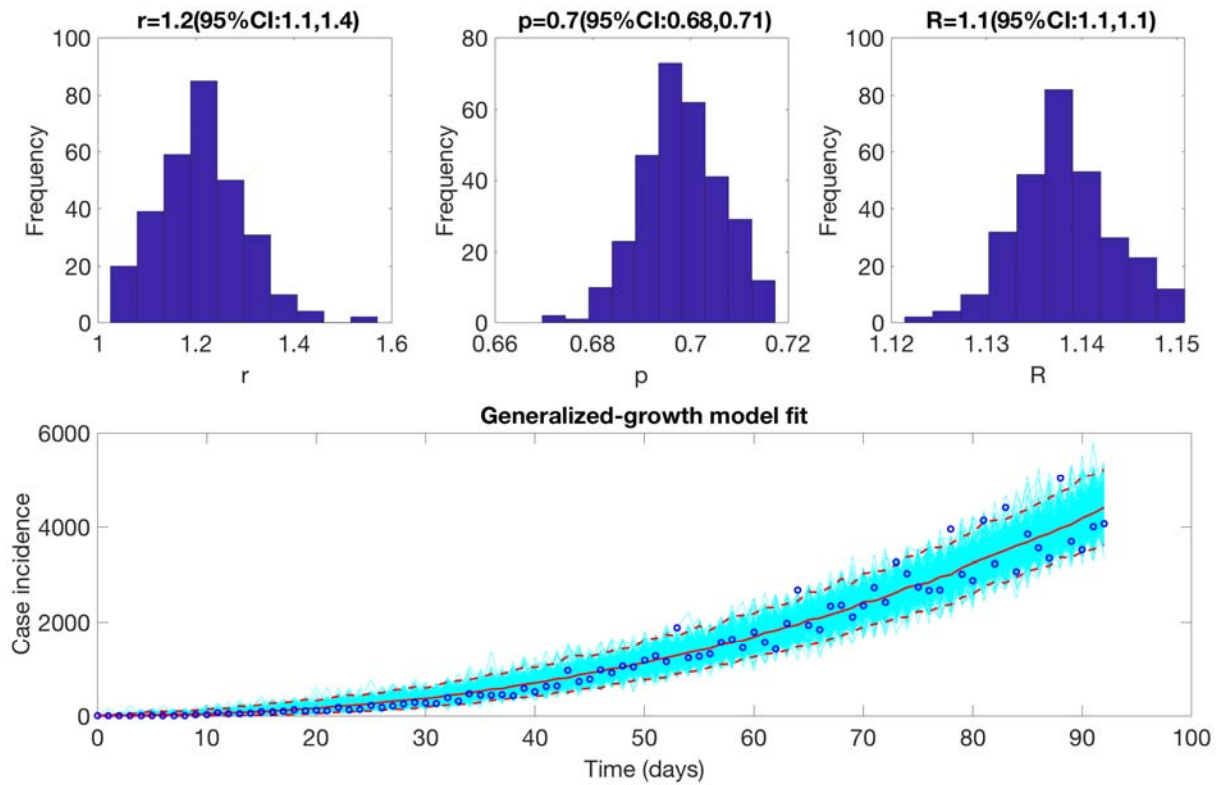
1315

1316   Fig 9: Upper panel: Reproduction number with 95% CI estimated using the GGM model. The estimated

1317   reproduction number of the COVID-19 epidemic in Mexico as of May 29, 2020, 2020 is 1.1 (95% CI:

1318   1.1, 1.1). The growth rate parameter, r, is estimated at 1.2(95%CI: 1.1, 1.4) and the deceleration of growth

1319   parameter, p, is estimated at 0.7 (95%CI:0.68, 0.71).

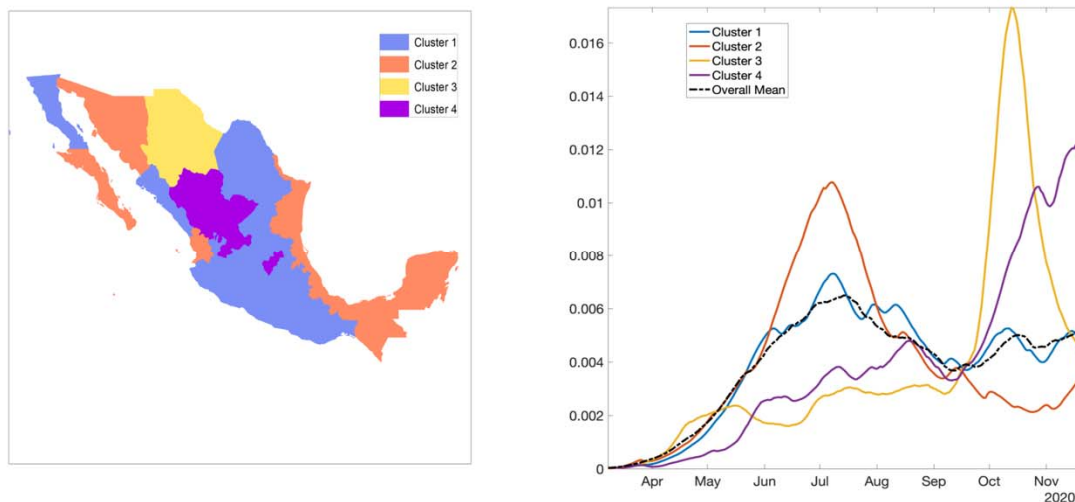1320   Lower panel: The lower panel shows the GGM fit to the case incidence data for the first 90 days.

1321

Fig 10: Upper panel: Epidemiological curve (by the dates of symptom onset) for Mexico (left panel) and Mexico City (right panel) as of September 27, 2020.

Lower panel: Instantaneous reproduction number with 95% credible intervals for the COVID-19 epidemic in Mexico as of September 27, 2020. The red solid line represents the mean reproduction number for Mexico and the red shaded area represents the 95% credible interval around it. The blue solid line represents the mean reproduction number for the Mexico City and the blue shaded region represents the 95% credible interval around it.
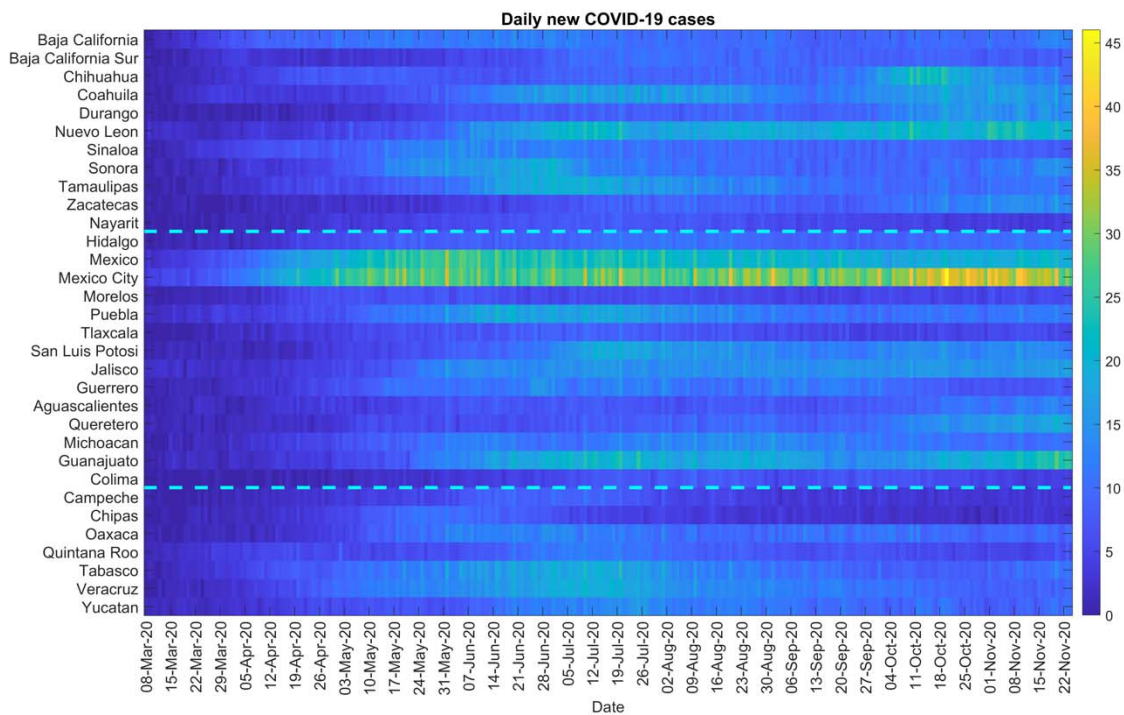
1335

1336

1337

1338

1339

1340   Fig 11: Clusters of states by their growth rates. Cluster 1 in blue, cluster 2 in orange, cluster 3 in

1341   yellow, and cluster 4 in purple. The right panel shows the average growth rate curves for each

1342   cluster (solid curves) and their overall average (black broken curve).

1343

Fig 12: Color scale image of daily COVID-19 cases by region.

1344

1345

1346

1347

1348

1349

1350

1351

1352

1353

1354

1355

1356

1357